

Copyright is owned by the Author of the thesis. Permission is given for a copy to be downloaded by an individual for the purpose of research and private study only. The thesis may not be reproduced elsewhere without the permission of the Author.

Appendix A.1. Thicknesses of substrate lithologies

This appendix is related to the information about the substrate beneath Auckland. The thicknesses and distribution of these lithologies, which are schematically and generically described in chapters 3, 5, 6, and 7 in the thesis, were taken principally from three sources in the literature: Kenny et al. (2011), Kenny et al. (2012), Kereszturi et al. (2014). In turn, these publications based their results in the use, analysis, and modelling of deep borehole data now in the PETLAB website (www.pet.gns.cri.nz). Apart from borehole data, Kenny et al. (2011, 2012) use geophysical data combined with structural information gleaned from current topography and exposed geology (the main objective of these authors was the mapping of unknown faults in the Auckland area). Since all authors have used a great deal of borehole data (Fig. A.1.1) (Kenny et al., 2011, 2012 used over 2000 borehole drill data and Kereszturi et al., 2014, used 421 borehole drill data), the specific borehole information will not be presented in this appendix. Instead the regional thicknesses of the lithologies in the southern volcanic field (Northern Manukau Lowlands or simply Manukau Lowlands) are shown in cross-sections and maps.

The presence of Waitemata rocks beneath North Head and Motukorea is attested by the exposures of this lithology around the volcanoes. North Head did not disrupt the underlying substrate (chapter 7), but Motukorea was erupted through 200-300 m of Waitemata substrate (chapter 6). The figures for the Waitemata thickness at Motukorea were also inferred from Kenny et al. (2011, 2012) data. The Auckland Volcanic Field (AVF) has been subdivided into the northern AVF (North Shore and Auckland Isthmus, Fig. A.1.1) and the southern AVF (Northern Manukau Lowlands, Fig. A.1.1). The former seats virtually on Waitemata rocks, whereas the latter overlies a combination of Waitemata rocks and Plio-Pleistocene sediments (Kaawa Formation + Tauranga Group) (see chapter 3 for descriptions of lithologies).

Fig. A.1.1 (figure modified from Kenny et al., 2012) shows the map of the Auckland region showing boreholes used in Kenny et al. (2011, 2012) study. Kereszturi et al. (2014) used boreholes located in the Manukau Lowlands. The locations of the studied volcanoes are shown.

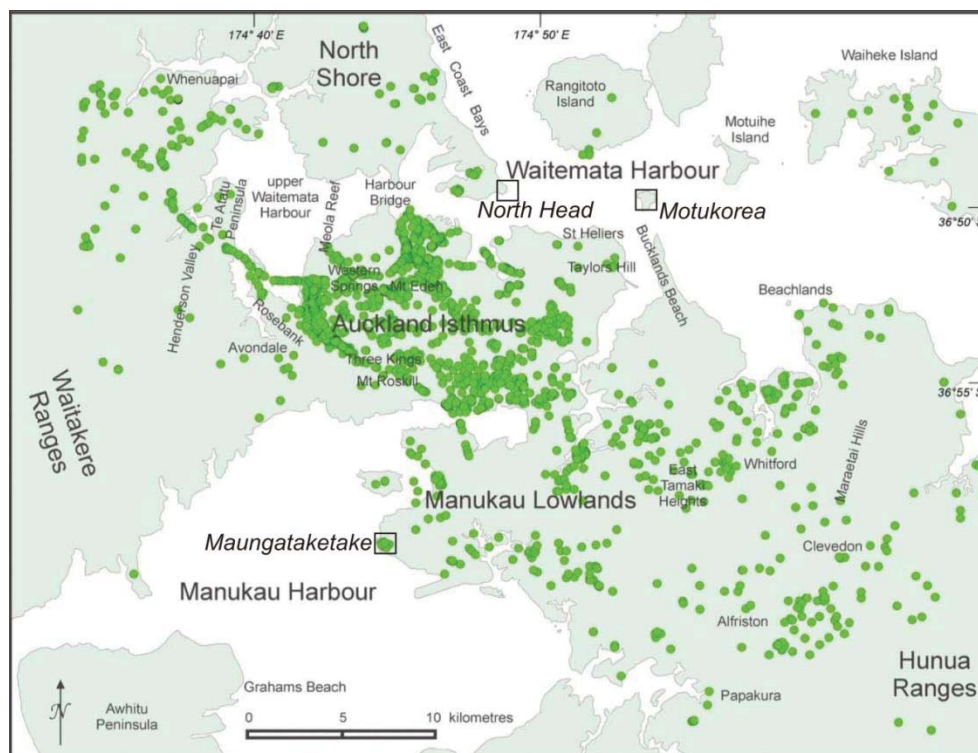


Fig. A.1.1

Fig. A.1.2 (from Kenny et al., 2012) shows the elevation map of current Auckland topography. It can be seen that the southern AVF is located in the low lying area known as the Manukau Lowlands.

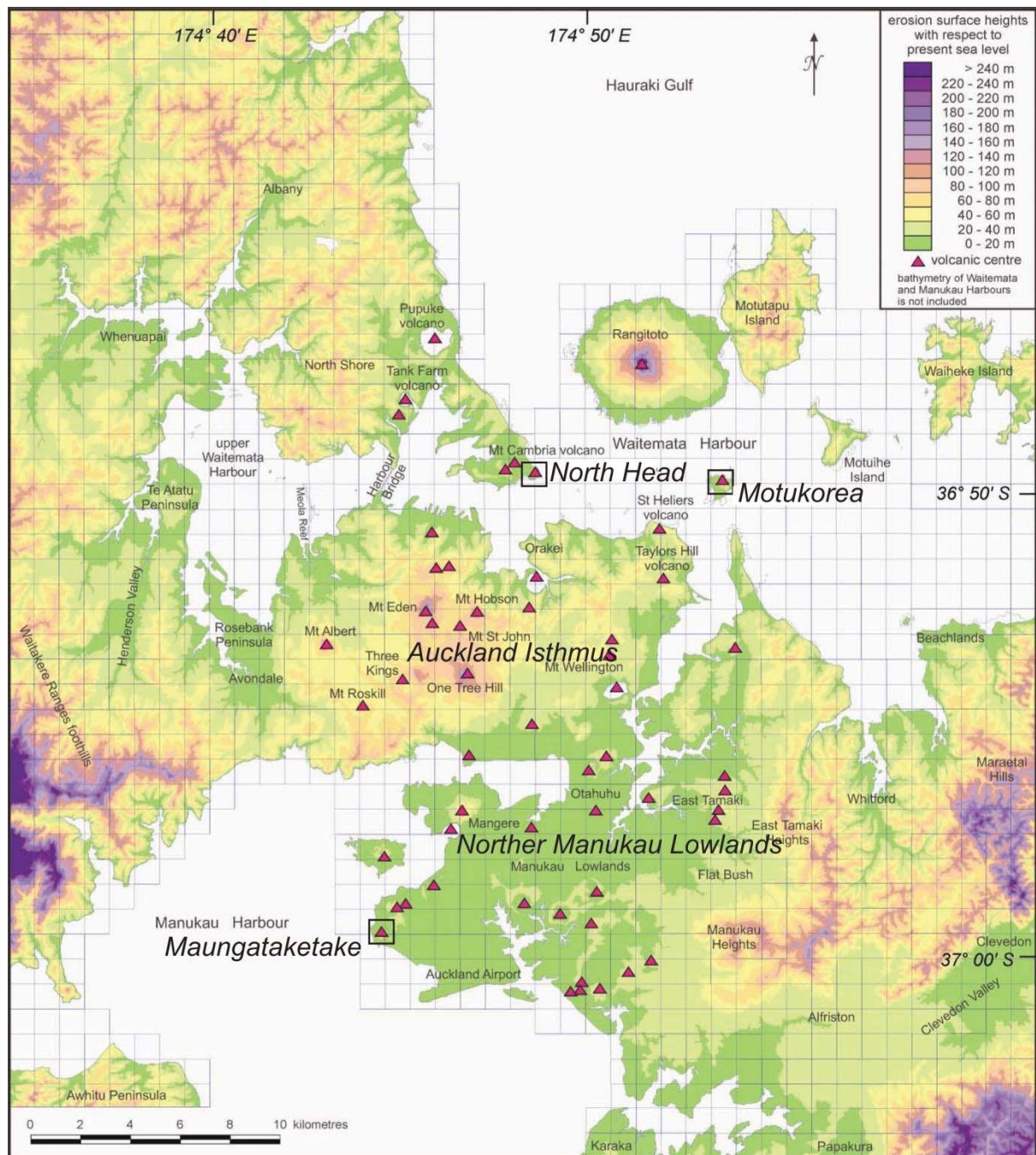


Fig. A.1.2

On the other hand, the erosion surface of the Waitemata Group rocks is now exposed or concealed beneath volcanics and sediments in the AVF. The erosion surface is the top of the Waitemata rocks as it exists at present time. Kenny et al. (2011, 2012) plotted the depths to the Waitemata Group from borehole log information and

This two previous map (2.1.2 and 2.1.3) give an idea of the distribution of the surface of the Waitemata rocks and its depth, which in turn provides clues on the type of the pre-eruptive surface at the time of the eruptions took place. This information was invoked in the reconstruction of the eruption of the three studied volcanoes.

According to Kenny et al. (2012) approximately 55% of the boreholes penetrated into the Waitemata rocks and further 5% reached the basement greywacke, either through the Waitemata rocks (and occasionally also Te Kuiti Group, see figure 3.2 in the main thesis text) or directly beneath superficial post-Miocene sediments. Of the remaining 40% just under half ended in post-Miocene sediments of fill. Due the relatively limited of drill holes reaching the basement, the thickness of the Waitemata Group rocks is difficult to assess. However, with the borehole information gathered and analysed by Kenny et al. (2011, 2012) it was possible to plot a map with locations of boreholes reaching greywacke (basement) (Fig. 2.1.4 from Kenny et al., 2011), where the depths are written in black numbers, or extending deep into Waitemata Group rocks without penetrating greywacke (grey numbers with a > 'deeper than' symbol). Greywacke is encountered in successively deeper boreholes in a westward direction (Fig. 2.1.4), but is deep under most of Auckland and yet to be penetrated (Kenny et al., 2011). Geophysical information analysed by Kenny et al. (2011) showed that the interface between the basement and the Waitemata rocks dips westward at different areas in the Auckland area. This information was used in chapter 6 to infer the thickness of the Waitemata rocks beneath Motukorea.

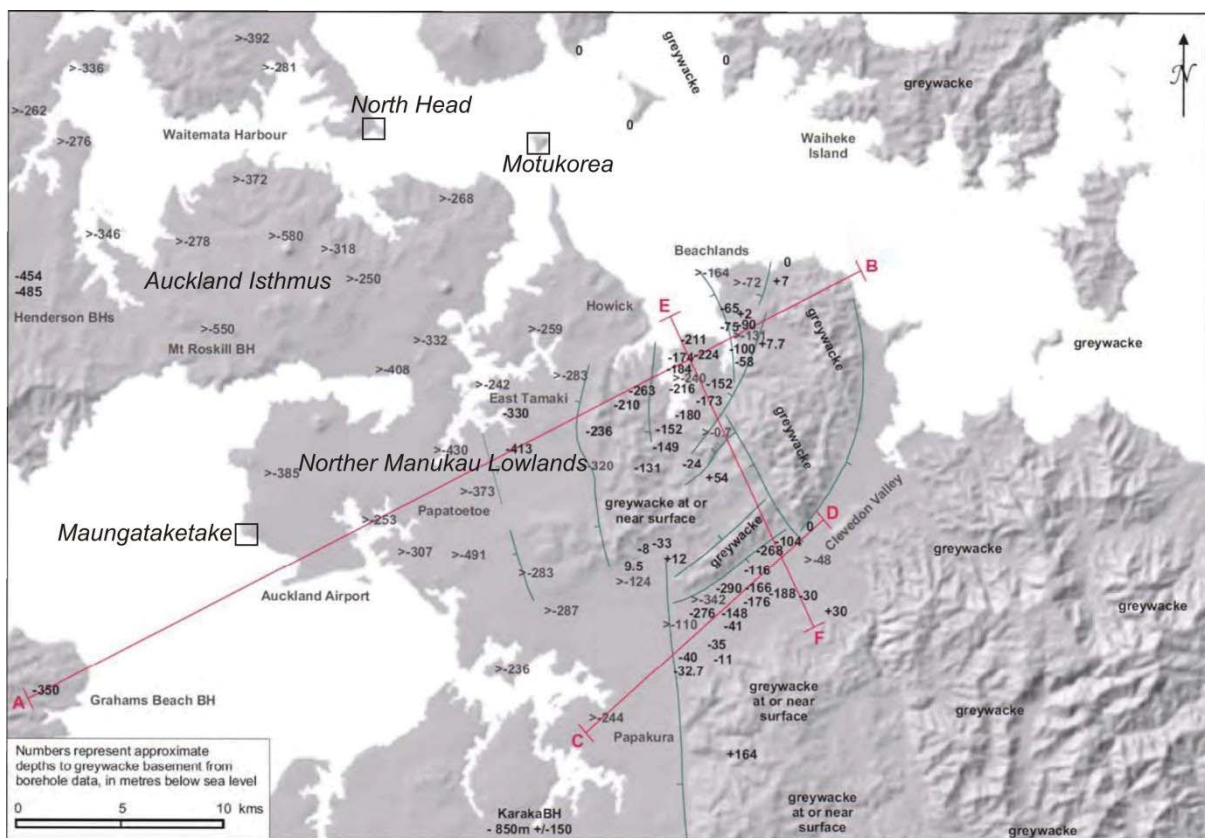


Fig. 2.1.4

A simplified cross-section A-B (Fig. 2.1.4) is shown in Fig. 2.1.5 (from Kenny et al., 2012). This cross-section corresponds to the Manukau Lowlands area and gives a general idea of the distribution of lithologies beneath the volcanics in this part of the AVF.

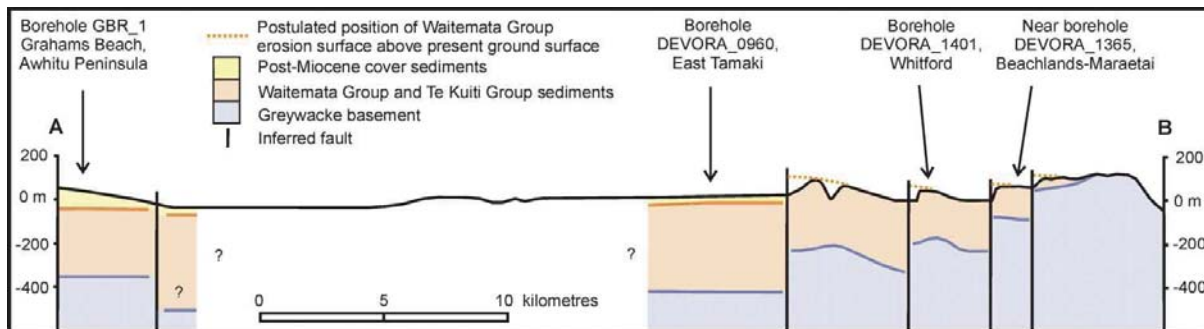


Fig. 2.1.5

The Plio-Pleistocene sediments, that is Tauranga Group and Kaawa Formation (see Fig. 3.2 and main thesis text in chapter 3 for description of such lithologies), are named Post-Miocene cover sediments by Kenny et al. (2012).

Kereszturi et al. (2014) presents a more detailed cross-section from the Manukau Lowlands (Fig. 2.1.6; modified from Kereszturi et al., 2014)). The maximum depth of the loose sediment cover (i.e. Tauranga Group and Kaawa Formation) at each drill core location was used to create an interpolated surface using natural neighbour interpolation method. In the AVF, the Manukau Lowlands host the largest thickness of post Waitemata soft-sediment cover within coastal alluvial basin. The cross-section are A-A' and B-B', both are within the Manukau Lowland areas. Unfortunately, none of the cross-sections cuts at Maungataketake volcano, but it provides with a clear picture of the distribution of substrate lithologies in the Manukau Lowlands. However, by extrapolating the thicknesses of the Tauranga Group from the borehole data, the thicknesses of these, water-saturated, unconsolidated sediments were mapped across the AVF (Fig. 2.1.7). Maungataketake lies in an area where the sediment cover is around 40-50 m. Note that the presence of the Tauranga sediments is scarce in the northern AVF. The Kaawa Formation is absent in the northern AVF, but still present in the southern AVF, and was not mapped. The thickness of the Kaawa formation in the Manukau Lowlands is variable, but probably of tens of metres. Kaawa Formation thickness beneath Maungataketake is unknown, but few drill holes attest the presence of lenses of Kaawa lithologies.

References

- Kenny, J.A., Lindsay, J.M., Howe, T.M., 2011. Large-scale faulting in the Auckland region. Institute of Earth Sciences and Engineering Report 1-2011.04, Auckland, New Zealand, 95 pp.
- Kenny, J.A., Lindsay, J.M., Howe, T.M., 2012. Post-Miocene faults in Auckland: insights from borehole and topographic analysis. *New Zealand J Geol Geophys*, 55: 323-343.
- Kereszturi, G., Nemeth, K., Cronin, S.J., Procter, J., Agustin-Flores, J., 2014. Influences on the variability of eruption sequences and style transitions in the Auckland Volcanic Field, New Zealand. *J Volcanol Geotherm Res*, 286: 101-115.

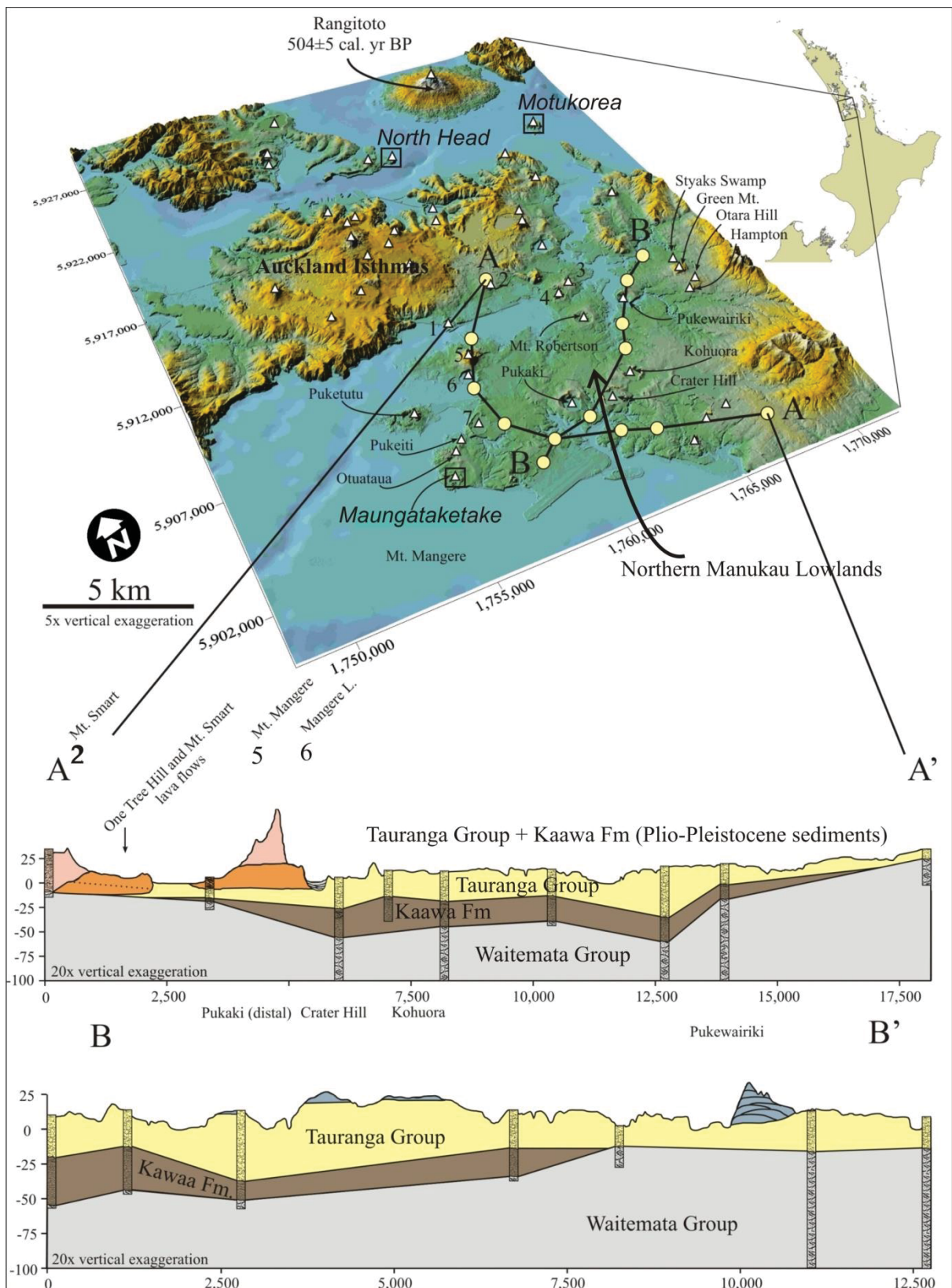


Fig. 2.1.6 The coordinates are in metres (New Zealand Transverse Mercator 2000).

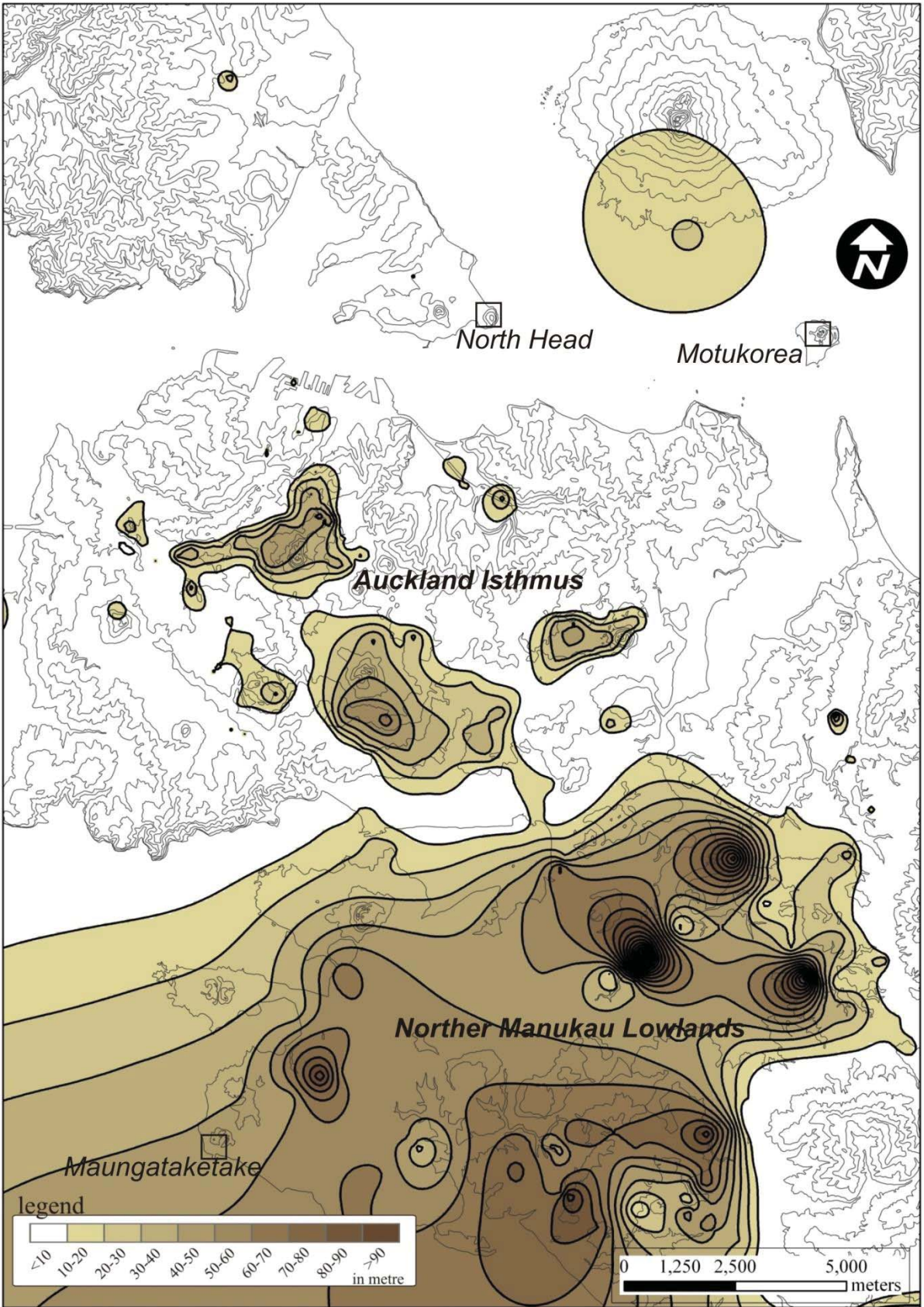


Fig. 2.1.7

Appendix A.2 Hydrogeological information

Some of the hydrogeological properties and aquifers characteristics of aquifers within the Auckland Volcanic Field are listed in Table A.1. All data is sourced from reports and unpublished data. Note that the widespread lava flows in the field form fractured aquifers.

References for the data on Table A.1:

- Auckland Regional Council, 1993: Draft Paraki geothermal groundwater resource statement and management plan.
- Crowcroft, G., Smaill, A., 2001. Auckland. In: Groundwaters of New Zealand. M.R. Rosen and P.A. White (Eds.). New Zealand Hydrological Society Inc., Wellington, New Zealand: 303-313.
- Crowcroft, G., Bowden, D., 2002. Auckland Water Resource Quantity Statement 2002; Surface water and groundwater resource information availability and location. Technical Publication Number 171, Auckland Regional Council, 44 pp.
- Harding, B.C., Pattle, A., Harris, M.G., Twose, G., 2010. Groundwater response to the dewatering of a volcanic vent. IAEG Congress 2010. Presentation, 15 pp.
- Moore, S.R., 1997. A combined geophysical and hydrogeological investigation of the Mt Richmond/McLennan Hills aquifer system, Auckland, New Zealand. M.Sc. thesis, The University of Auckland, 141 pp.
- Namjou, P., 1996. Hydrogeological evaluation of proposed landfill sites in the greater Auckland area (New Zealand): Mt Wellington and Peach Hill Valley. M.Sc. thesis, The University of Auckland, 479 pp.
- Namjou, P., Strayton, G., Pattle, A., Davis, M.D., Kinley, P., Cowpewartait, P., Salinger, M., Mullan, A., Patterson, G., 2005. Groundwater behavior in a fractured basalt aquifer under existing and future climate and land use in Auckland City (New Zealand). Impacts of Global Climate Change: 1-12.
- Orgias, S., 2004. Groundwater flow characteristics of a low lying coastal aquifer system, Okahukura Peninsula, North Auckland. M.Sc. thesis, The University of Auckland, New Zealand,
- Scoble, R. and Millar, A., 1995. Kumeu-Hobsonville groundwater resource assessment report (TP60). Auckland Regional Council (now Auckland Council) Technical Publication, Auckland Council, New Zealand, 70 pp.
- Sheridan, G.J., 2006. The macroporosity and microporosity components of the Waitemata group rocks, Auckland, New Zealand. M.Sc. thesis, The University of Auckland, New Zealand, 105 pp.
- Viljevac, Z., 1998. Western Springs Aquifer. Hydrogeological characteristics and computer model. M.Sc. thesis, The University of Auckland, 144 p.
- Viljevac, Z., Murphy, G., Smaill, A., Crowcroft, G., and Bowden, D., 2002. South Auckland groundwater, Kaawa aquifer recharge study and management of the Volcanic and Kaawa aquifers. Auckland Regional Council (now Auckland Council) Technical Publication, Auckland Council, New Zealand, Number 133, 193 pp.

Table A.1

Aquifer	Aquifer type	Locality	Thickness (m)	Porosity	Permeability
Waitemata	Confined/semiconfined	General	200-400 (?) depth of bores		
Auckland volcanics	Fractured, unconfined	Onehunga/Mt Wellington	<60		
Auckland volcanics	Fractured, unconfined	Western Springs	<50		
Auckland volcanics	Fractured, unconfined	Mt Richmond	<45		
South Auckland volcanics	Fractured, unconfined (?)	General	Boreholes drilled 30-60		
Kaawa	Confined porous	General	Shellbeds (Up to 6 m)		
Waitemata	Confined to semiconfined (?)	North-Western Region	Bores drilled 120-300		
Waitemata	Confined to semiconfined (?)	North-East Region (General)	100-800		
Waitemata	Confined to semiconfined (leaky)	North-East Region (Taramata)	100-150		
Waitemata	Confined to semiconfined (?)	Kaipara and North Shore Region	Boreholes drilled 50-370		
Auckland volcanics	Unconfined	One Tree Hill	<60		
Auckland volcanics	Unconfined	Mt Wellington-Mt Smart			
Auckland volcanics	Unconfined	Western Springs	<50		
Auckland volcanics	Unconfined	Mt Richmond	<45		
Auckland volcanics	Unconfined	McLaughlins/Wiri	<30		
Waitemata	Confined to semiconfined (?)	Manukau/Wiri	>500		
Waitemata	Confined to semiconfined (?)	East Tamaki	Up to 600		
Waitemata	Confined to semiconfined (?)	Clevedon East	Up to 230		
Waitemata	Confined to semiconfined (?)	Clevedon West	Up to 300		
Waitemata	Confined (?)	South Auckland area			
Auckland volcanics	Unconfined	Mt Wellington			3x10E-6-1x10E-3 m/s
Waitemata	Semiconfined	General			
Waitemata	Semiconfined	Three Kings (A) [Disturbed]			
Waitemata	Semiconfined	Three Kings (A) [Undisturbed]			
Waitemata	Semiconfined (?)	Bitomart	30 m (for practical purposes)		
Auckland volcanics	Unconfined	Three Kings			
Waitemata	Semiconfined (?)	Kumeau-Hobsonville	>300		
Auckland volcanics	Unconfined-perched	Basallic, South Auckland	up to 100	Primary (up to 10%) Actual (>25%)	
Tuff	N/A	South Auckland area		Welded (14%) Pumiceous (40%)	
Plio-Pleistocene sediments	N/A	South Auckland area			
Kaawa	Confined	South Auckland area	up to 240		
Waitemata	Confined-perched	South Auckland area			
Auckland volcanics	Unconfined-perched	South Auckland area (?)			
Kaawa	Confined-perched	South Auckland area (?)			
Waitemata	?	South Auckland area (?)			
Waitemata	Fractured (?)	Paraki			
Auckland volcanics	Fractured	Auckland area	38.3, 24, 34.3		
Waitemata	Fractured (?)	Omaha Beach			
Auckland volcanics	Fractured (?)	McLennan Hills	up to 45		
Auckland volcanics	Fractured (?)	Mt Richmond			
Auckland volcanics	Fractured (?)	General			
Auckland volcanics	Fractured (?)	Onehunga (Royal Oak)			
Auckland volcanics	Fractured (?)	Onehunga (Penrose)			
Auckland volcanics	Fractured (?)	Onehunga (Mt Wellington)			
Auckland volcanics	Fractured (?)	Onehunga (Sauldrown)			
Auckland volcanics	Fractured (?)	Western Springs (Mt Eden)			
Auckland volcanics	Fractured (?)	Western Springs (Three Kings)			
Auckland volcanics	Unconfined, fractured	Mt Wellington	at least 40	effective poros= 0.08 +/- 0.02	
Auckland volcanics	Unconfined, fractured	Mt Wellington	at least 40	effective poros= 0.08 +/- 0.02	
Waitemata	Confined-unconfined	Mt Wellington (Waitemata)	100 m for study purposes (local aquifer system; but deeper	ave. effective poros= 0.3; siltstone and sandstone 0.01-0.4	
Waitemata	Confined-unconfined	Mt Wellington (siltstone)	100 m for study purposes (local aquifer system; but deeper	ave. effective poros= 0.3; siltstone and sandstone 0.01-0.4	
Plio-Pleistocene sediments	N/A	Mt Wellington	up to 10	non-permeable	
Alluvial deposits	N/A	Western Springs	up to 20	25-60%	10-100 darcy's
Tuff	N/A	Western Springs	up to 21 (two parts)	39, 40, 36, 14 %	0.04, 11.5, 1.4, 0.33 mDarcy's
Auckland volcanics	Unconfined	Western Springs			
Waitemata	Unconfined-semiconfined	Okahukura Peninsula			
Waitemata	Confined	ECBF/BHBF	outcrops, (305 measured)	effective porosity (sandstone)= 15.5%	

Appendix B.1 Maungataketake stratigraphic logs, frequency histograms, and volume percentage values of phi fractions of 12 selected samples.

This appendix first presents the total of logs corresponding to Maungataketake volcano (Figs. B.1.1 to B.1.9). There are 3 extra logs included (MM1, MM2, and MM3). The logs showed in chapter 5 (M1, M2, M3, M4, and M5) are also included. Additionally, because Fig. 5.2 is not clear in the thesis, the correlation of logs is presented as Fig. B.1.10 without the frequency histograms (now included in the logs) and the graph with the percentages of grain size fractions (now presented as itself in Fig. B.1.11). Also, Table B.1.1 displays the volume percentage for phi fractions of the 12 selected sieved samples.

Fig. B.1.1 shows the plan view of Maungataketake volcano (modified from Brand et al., 2014). Alongside the 5 sites described in chapter 5, other 3 sites are included.

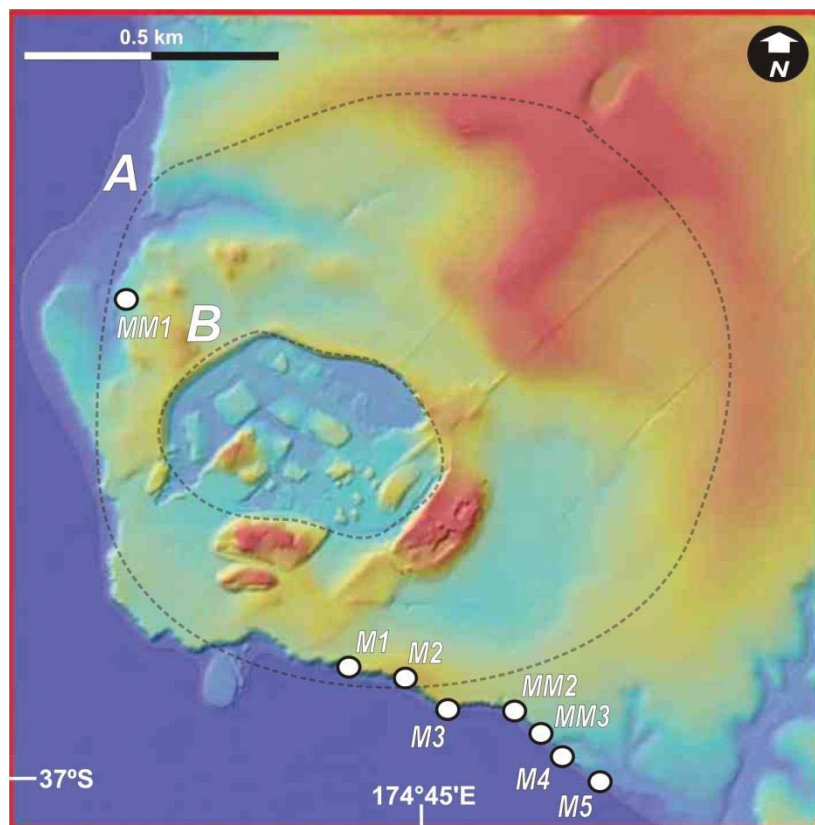


Fig. B.1.1 Location of sites

The stratigraphic logs are presented in the order showed in Fig. B.1.1, from NW to SE. Except for exposures at sites M1 (3 metres above back beach level) and M2 (5 metres above back beach level), all exposures are virtually at back beach level. The scale at each log indicates thickness of exposures. A brief description of exposures is included. Specific descriptions of lithofacies are shown in Table 5.2 in the main text. A correlation and identification of units was not possible for site MM1. The letters at the upper right corner of some figures included in the main text are kept for identification in Fig. 5.5 in the main text. All histograms show grain size distribution of fine tuff and the sample number on histograms corresponds to the 12 sample numbers on Table B.1.1 and Fig B.1.11. Sample number on histograms is located at the upper left section (M followed by a number)

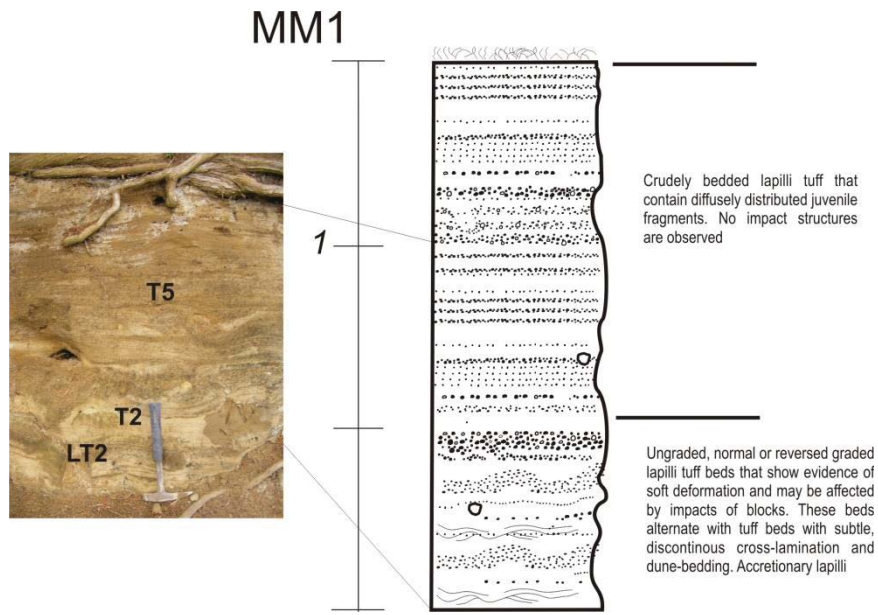


Fig. B.1.2 Site MM1 (at back beach level)

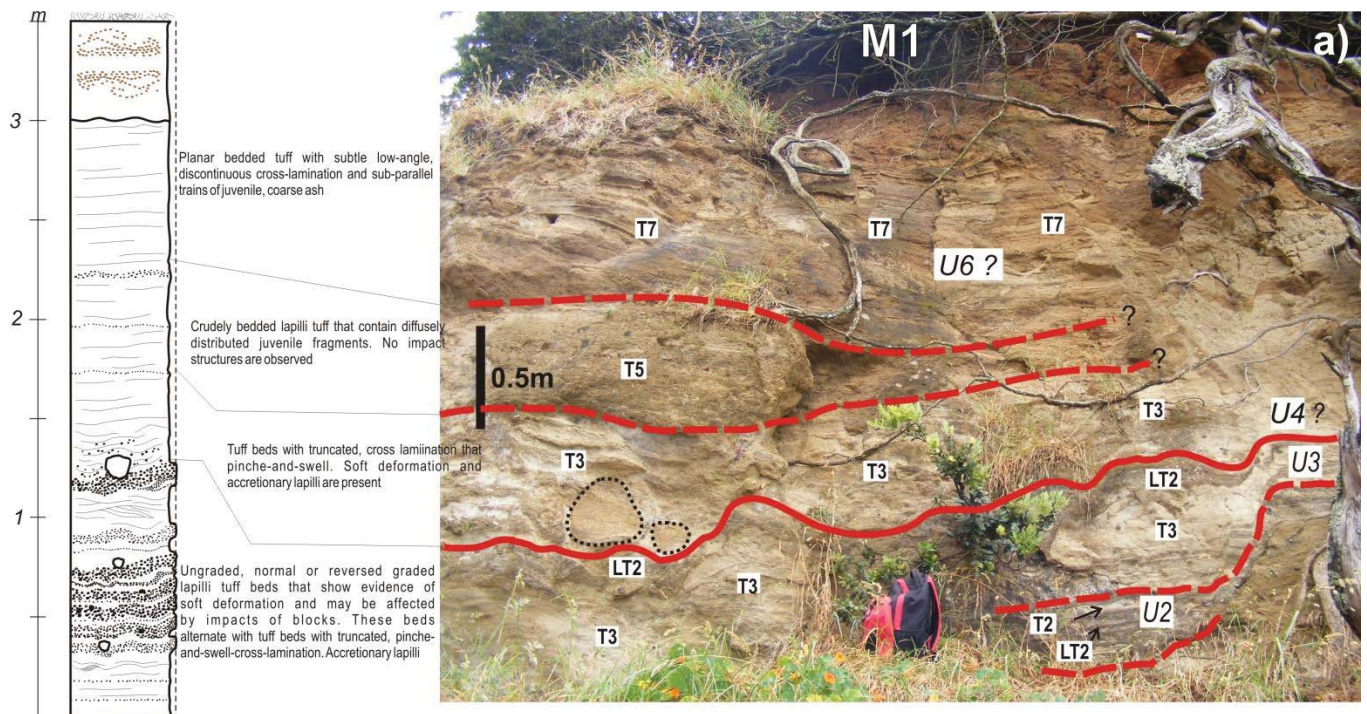


Fig. B.1.3 Site M1. (3 metres above back beach level)

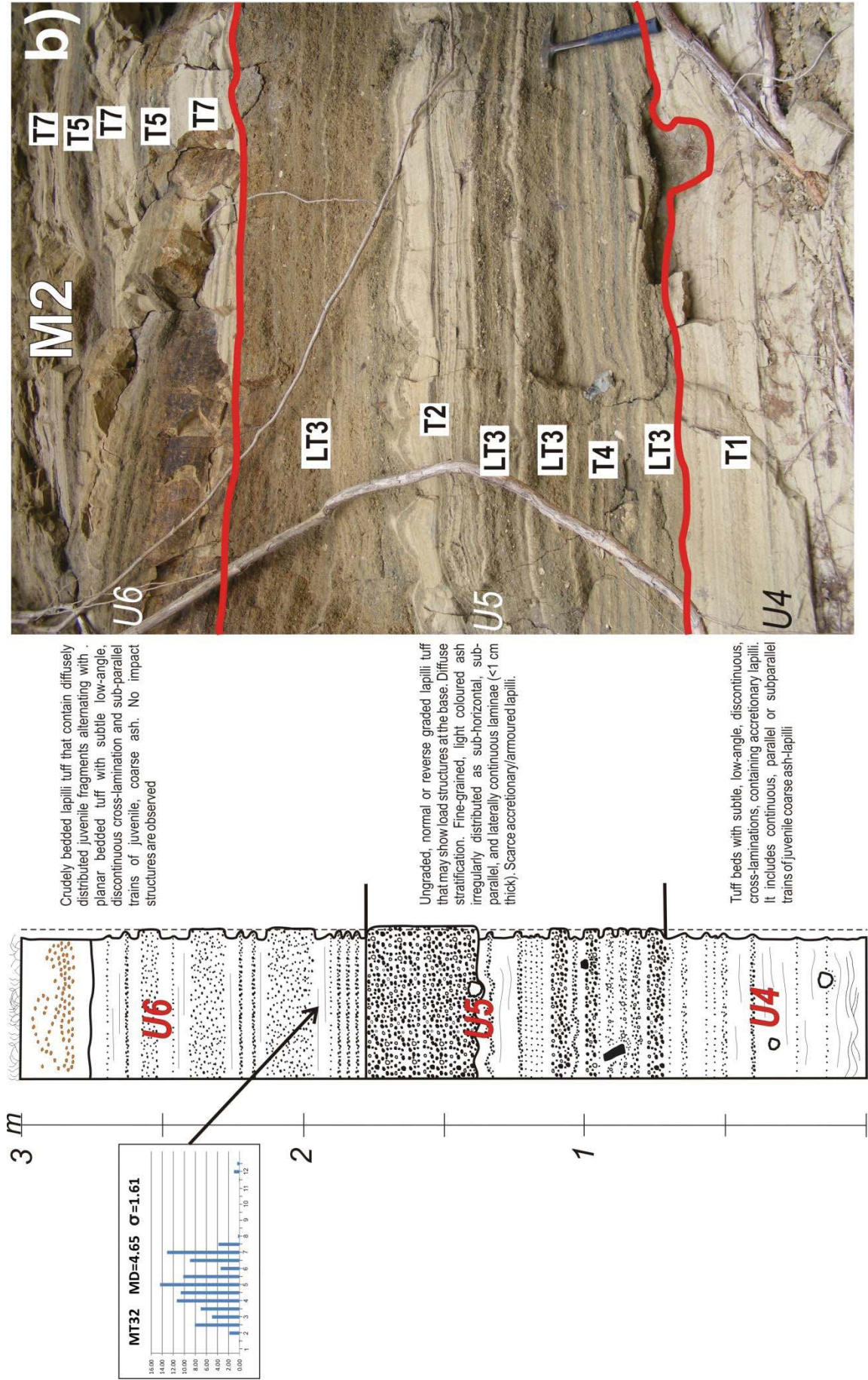


Fig. B.1.4 Site M2 (at 5 metres above back beach level).

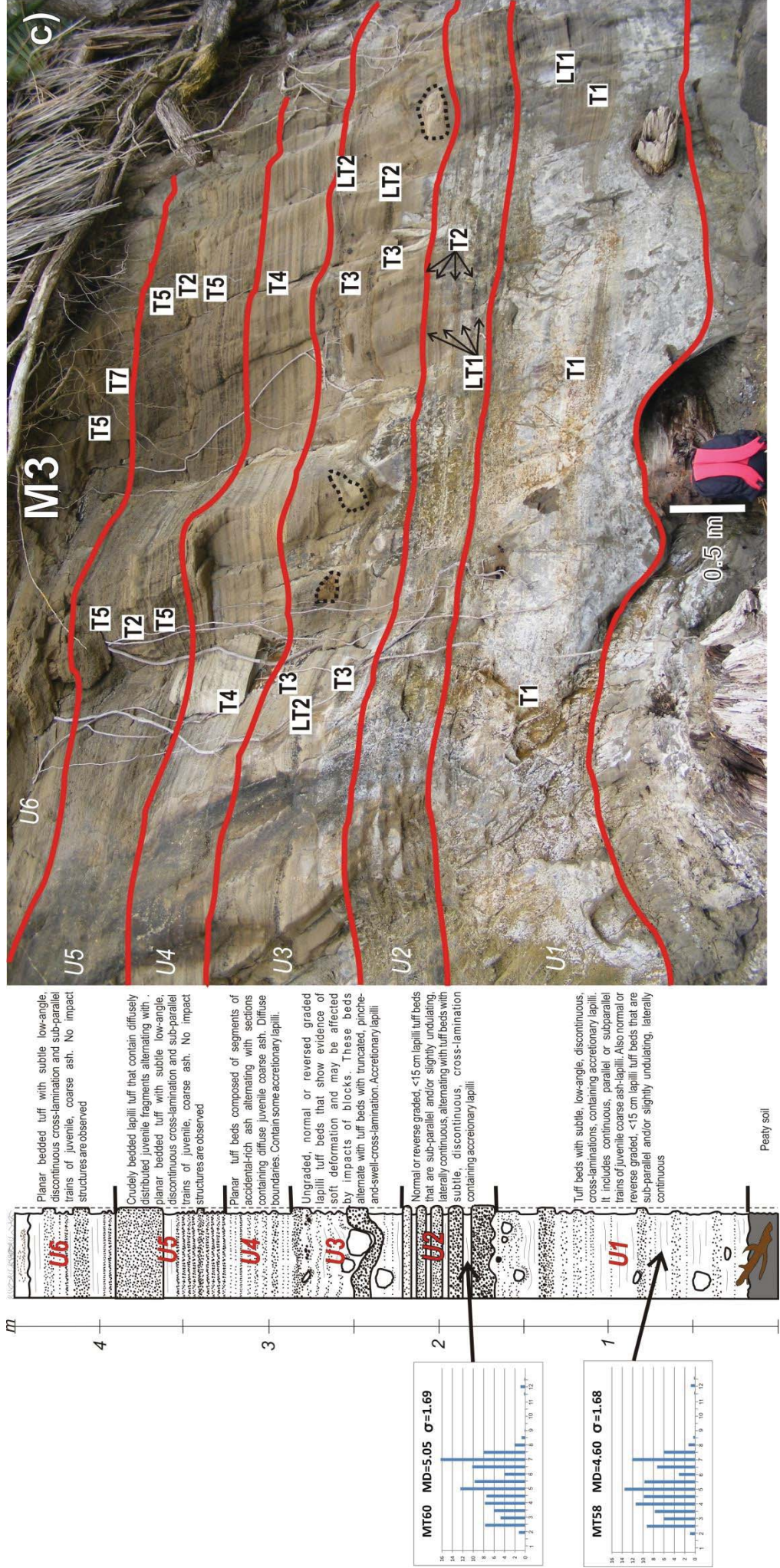


Fig. B.1.5 Site M3 (at back beach level)

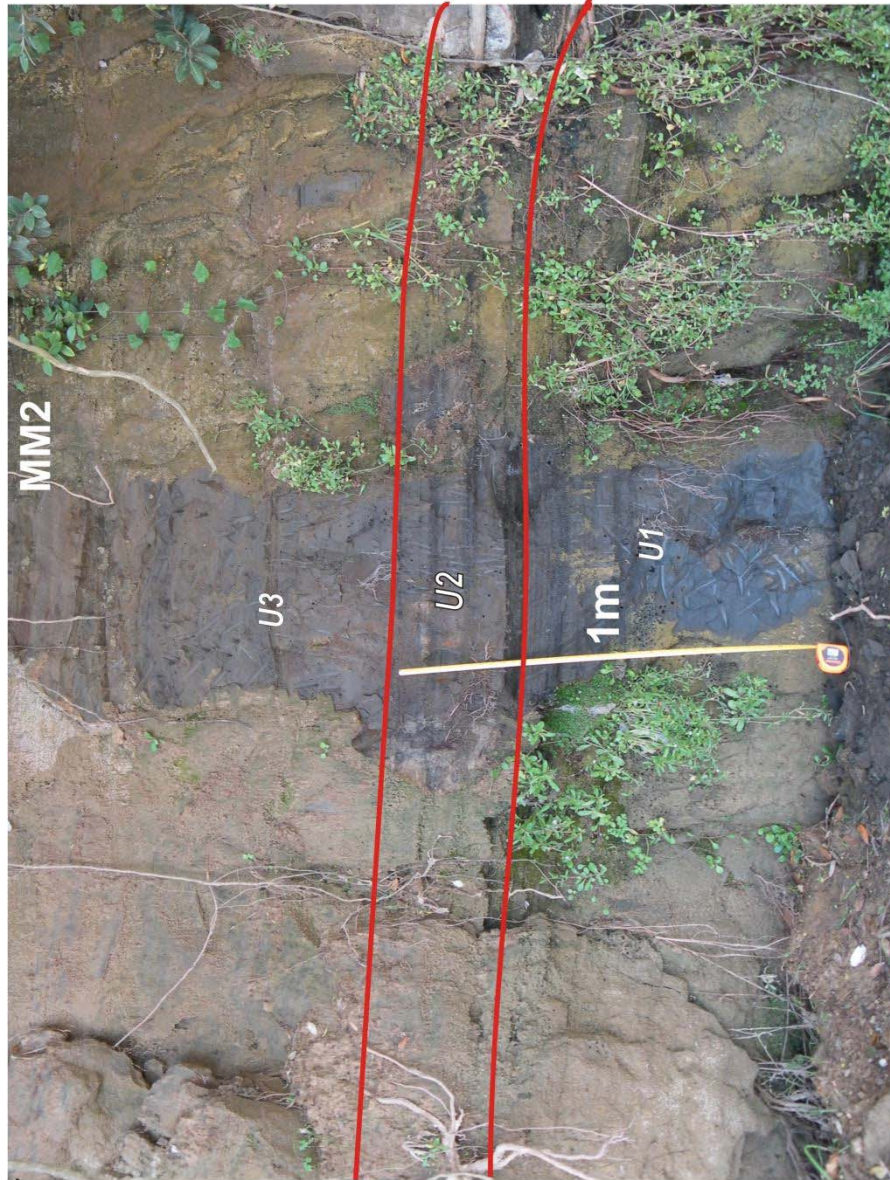
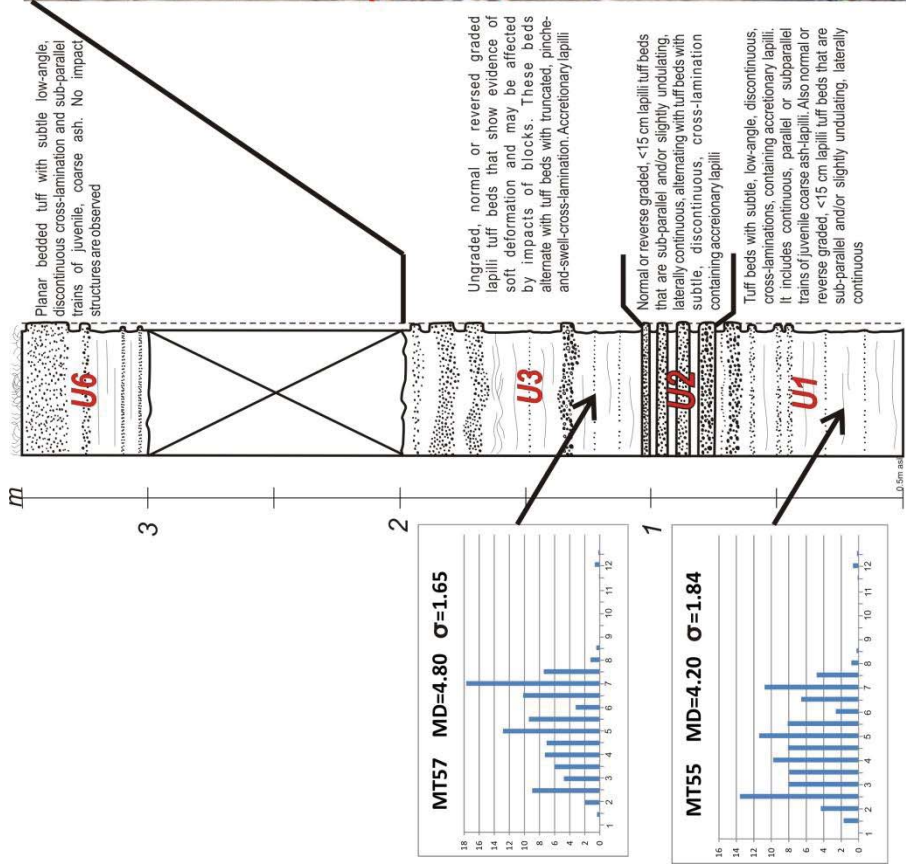
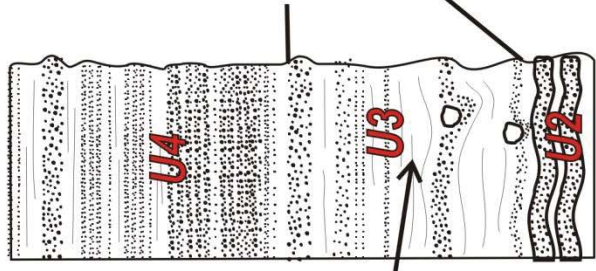
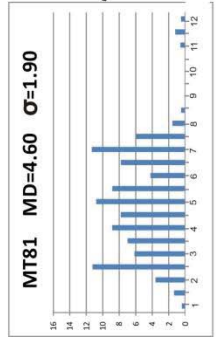


Fig. B.1.6 Site MM2 (at back beach level)

m

1



Planar beds that consists of layers of fine grained ash of accidental origin alternating with juvenile-rich layers arranged in trains or thin beds of irregular thickness (from few mm to up to 3 cm). Subtle soft deformation and abundant accretionary lapilli.

Ungraded, normal or reverse graded lapilli tuff that may show load structures at the base. Diffuse stratification, alternating with fine-grained, light coloured ash irregularly distributed as sub-horizontal, sub-parallel, and laterally continuous laminae. Accretionary lapilli.

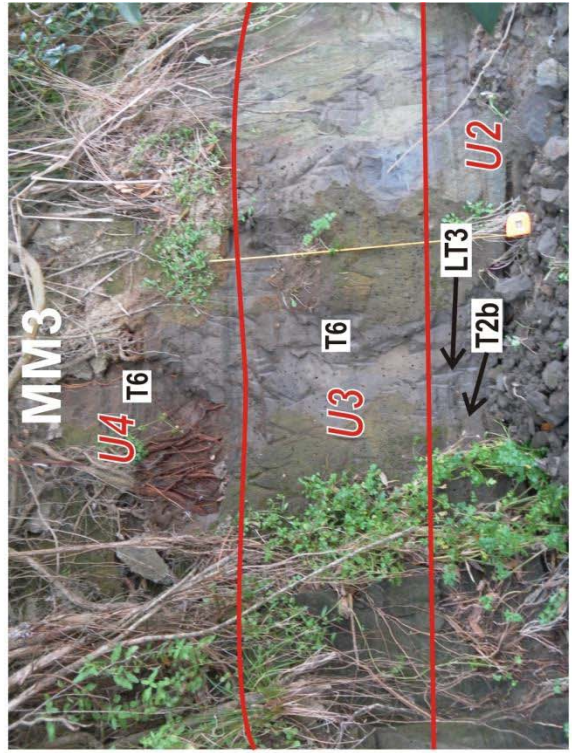


Fig. B.1.7 Site MM3 (at back beach level)

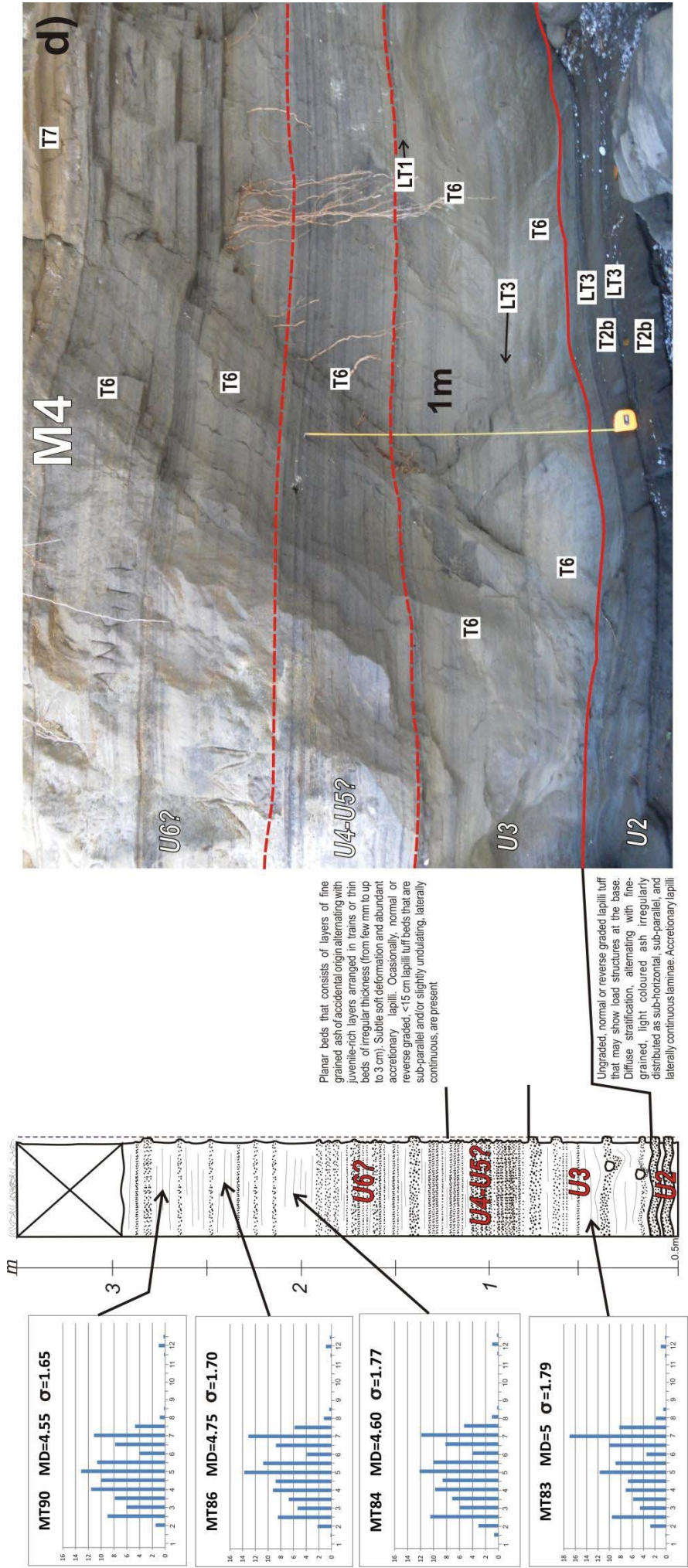


Fig. B.1.8 Site M4 (at back beach level)

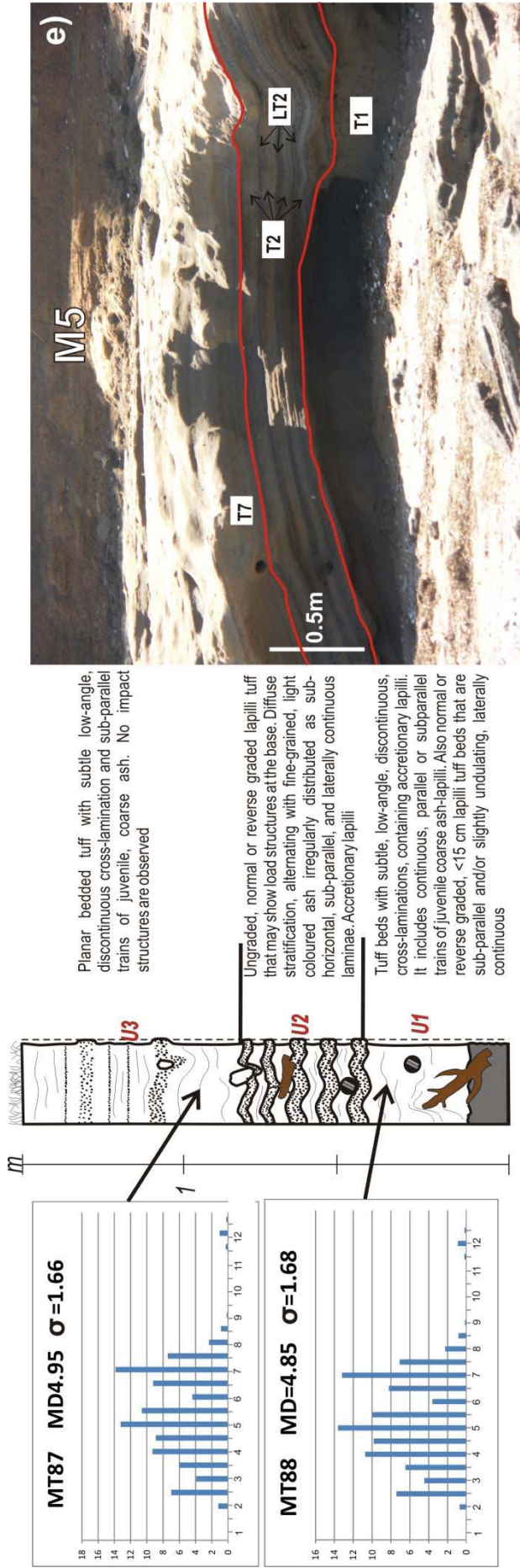


Fig. B.1.9 Site M5 (at back beach level)

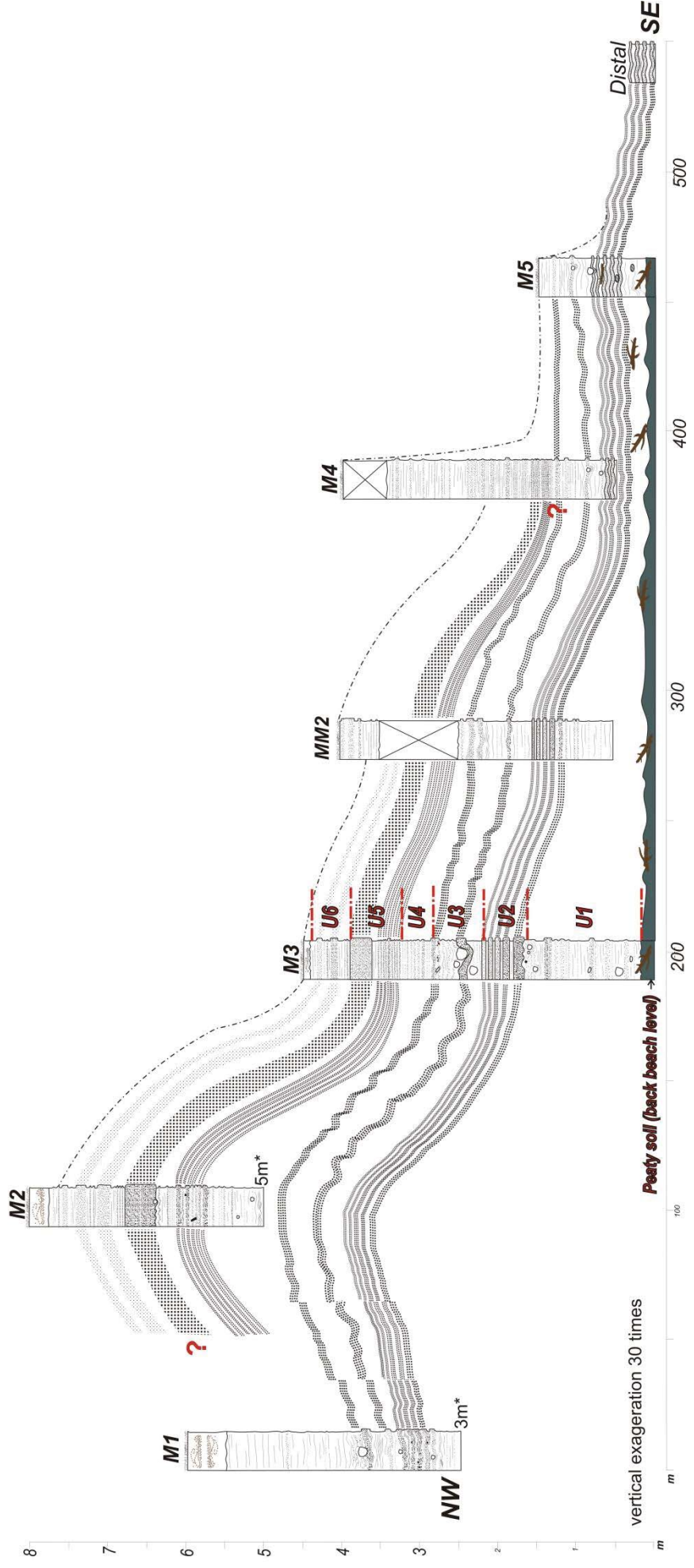


Fig. B.1.10 Schematic correlation of logs and identified units. Note that site MM1 (Fig. B.1.2) is not included. Site MM3 (Fig. B.1.7) is located next to site M4. This correlation represents an approach of the cross-section of the ejecta ring from NW to SE. The vertical axis represents the maximum thickness of the exposed sequence. The peaty soil, when exposed, is at the base of the phreatomagmatic deposits and corresponds to the back rim, whereas Site M2 is located at the crater rim, whereas Site M1 is located at the inner slope of the ejecta ring.

Table B.1.1 displays the volume percentage values for phi fractions of the 12 sieved samples. The sample number is the same on the histograms shown with the logs and the graph of figure B.1.11

Grain size	Phi	Sample / vol.%											
		MT32	MT55	MT57	MT58	MT60	MT81	MT83	MT84	MT86	MT87	MT88	MT90
	1	0.00	0.06	0.02	0.00	0.00	0.41	0.00	0.01	0.00	0.00	0.00	0.00
	1.5	0.13	1.72	0.37	0.00	0.00	1.35	0.16	0.68	0.18	0.00	0.00	0.00
Coarse ash		0.13	1.78	0.39	0.00	0.00	1.76	0.16	0.69	0.18	0.00	0.00	0.00
	2	1.87	4.35	1.96	0.98	1.24	3.61	2.81	3.09	2.21	1.20	0.72	1.50
	2.5	8.09	13.59	8.98	9.28	7.74	11.25	9.54	10.52	8.46	7.00	7.43	9.02
	3	5.00	8.04	4.78	6.04	4.75	6.15	4.64	5.97	5.35	3.92	4.47	6.07
	3.5	7.03	7.93	6.01	7.75	5.99	7.00	5.82	7.14	6.75	5.97	6.47	7.87
	4	11.39	9.80	7.30	11.42	7.78	8.87	7.13	9.78	9.24	9.31	10.74	11.59
Medium ash		33.37	43.71	29.02	35.47	27.50	36.88	29.94	36.49	32.00	27.40	29.83	36.05
	4.5	10.65	8.11	7.06	9.85	7.45	7.82	6.73	8.60	8.80	8.90	9.83	10.03
	5	14.40	11.39	12.85	13.56	12.47	10.80	11.71	12.16	13.74	13.22	13.62	13.13
	5.5	10.19	8.13	9.41	9.75	9.73	8.84	8.93	10.04	10.76	10.61	9.99	10.62
	6	3.43	2.62	3.20	3.12	3.97	4.23	3.48	3.98	3.89	4.39	3.62	4.01
	6.5	8.98	6.59	10.17	7.29	10.18	7.80	9.97	8.17	8.76	9.24	8.22	7.82
	7	13.13	10.77	17.71	12.10	16.30	11.34	17.01	11.88	13.10	13.87	13.19	11.12
	7.5	3.83	4.81	7.45	5.94	8.01	5.97	8.24	5.30	5.83	7.42	7.08	4.71
Fine ash (silt)		64.61	52.43	67.85	61.62	68.11	56.80	66.06	60.13	64.89	67.66	65.55	61.44
	8	0.31	0.84	1.25	1.27	2.09	1.55	1.82	1.01	1.21	2.35	2.25	0.83
	8.5	0.00	0.25	0.46	0.35	0.73	0.50	0.54	0.23	0.36	0.87	0.84	0.20
	9	0.00	0.03	0.06	0.04	0.15	0.05	0.07	0.00	0.04	0.17	0.17	0.00
	9.5	0.00	0.00	0.00	0.00	0.00	0.00	0.00	0.00	0.00	0.00	0.00	0.00
	10	0.00	0.00	0.00	0.00	0.00	0.00	0.00	0.00	0.00	0.00	0.00	0.00
	10.5	0.00	0.00	0.00	0.00	0.00	0.00	0.00	0.00	0.00	0.00	0.00	0.00
	11	0.00	0.00	0.00	0.00	0.00	0.59	0.00	0.00	0.00	0.00	0.00	0.00
	11.5	0.13	0.12	0.11	0.17	0.25	1.20	0.23	0.21	0.17	0.29	0.23	0.20
	12	1.02	0.66	0.66	0.85	0.95	0.52	0.96	0.98	0.89	1.04	0.91	1.01
	12.5	0.43	0.20	0.20	0.23	0.21	0.09	0.23	0.25	0.25	0.22	0.21	0.28
	13	0.00	0.00	0.00	0.00	0.00	0.00	0.00	0.00	0.00	0.00	0.00	0.00
Fine ash (clay)		1.89	2.09	2.73	2.91	4.39	4.50	3.84	2.68	2.93	4.95	4.62	2.51

Table B.1.1

With data from the grain size analyses, the phi fractions were plotted in regard to grain size classification. Note that all samples exhibit the prevalence of fine ash.

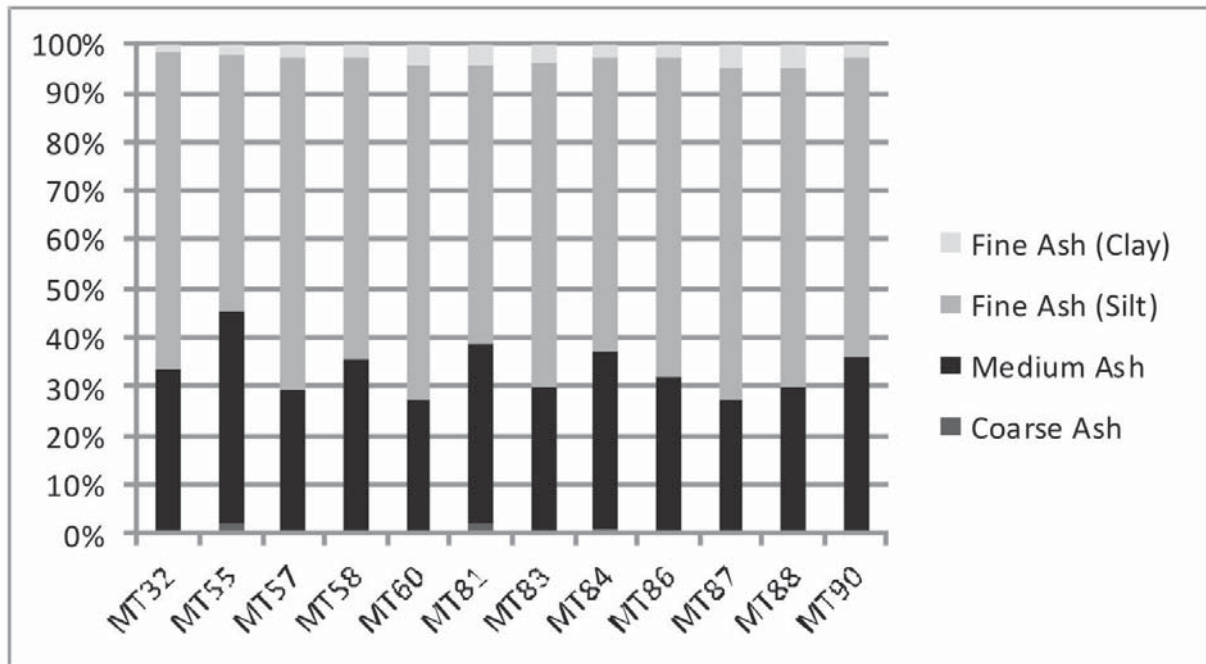


Fig. B.1.11

Appendix B.2 Lithofacies and units of Maungataketake volcano

1. LITHOFACIES

The sedimentary criteria to group and describe the lithofacies are provided in chapter 5. The referred figures for lithofacies are also displayed in chapter 5. The summarized information of these lithofacies is presented in Table 5.2 in chapter 5.

Tuff:

T1 (Figs. 5.5c,b,e; 5.6a,b,f). Poorly consolidated, faintly laminated to massive, grey tuff sequences that have variable thickness (up to 0.5 m). It is poorly sorted and composed mainly of fine ash (~ up to 55 vol.%) and medium ash (~ up to 35 vol.%) of accidental origin. It contains continuous, parallel/sub-parallel trains composed of juvenile, coarse ash (<1 mm) (<10 vol.%). Randomly, at intervals, the juvenile fragments coarsen (up to fine-lapillus size) and are sparsely concentrated in bands (up to 10 cm thick) that exhibit vague inverse gradation. Subtle low-angle, discontinuous cross-lamination and dune bedding is present at intervals. <5 mm-diameter, spherical/oval accretionary lapilli are displayed along discontinuous horizontal trains at some segments or else scattered randomly in the tuff, but it is not pervasive. Small block/medium lapillus-size fragments of accidental origin are relatively scarce (<5 vol.%) and they are embedded in the tuff or forming impact structures. The finer ash is composed of quartz, feldspar, and smaller amounts of clay; the coarser juvenile grains consist of basaltic glass (tachylite or sideromelane) with some, individual or clustered, olivine/pyroxene phenocrysts and abundant Ca-rich pyroxene microlites/microcrysts.

Interpretation: Soft deformation, poor sorting and the presence of accretionary lapilli point to deposition of wet base surges. The presence of juvenile trains of variable thickness suggests transportation of the diluted PDCs as a combination of weak-turbulent suspended loads and bed loads/traction-carpet. With distance, the base surges may have become less concentrated and deposition is related to suspension. (Sohn, 1997; Sohn and Chough; 1989; Chough and Sohn, 1990).

T2 (Figs. 5.5a,b,c,d,e; 5.6a,b,c,d,e,f). Poorly consolidated, faintly laminated, grey to light brown, tuff beds up to ~10 cm in thickness. Poorly sorted and composed mainly of fine ash (~ up to 55 vol.%) and medium ash (~ up to 35 vol.%) of accidental origin. It contains parallel to subparallel trains composed of juvenile coarse ash (<1 mm) (<10 vol.%). Subtle cross-lamination is observed at times. Rare accretionary lapilli (<5 mm in diameter) is present. The finer ash is composed of quartz, feldspar, and smaller amounts of clay; the coarser juvenile grains consists of basaltic glass (tachylite or sideromelane) with some, individual or clustered, olivine/pyroxene phenocrysts and abundant Ca-rich pyroxene microlites/microcrysts.

Interpretation: Soft deformation, poor sorting, accretionary lapilli, subtle cross-lamination, and thin trains of juvenile fragments suggest the deposition of wet base surges transported as a low-energy, suspended load. T2 is associated with the deposition of LT2 probably as a bipartite base surge. (Sohn, 1997; Sohn and Chough; 1989; Chough and Sohn, 1990; Vazquez and Ort, 2006).

T3 (Figs. 5.5a,c; 5.6a,b,d,g). Poorly consolidated, faintly laminated, grey to light brown tuff sequences of variable thickness (up to 0.5 m). Poorly sorted and composed mainly of fine ash (~ up to 55 vol.%) and medium ash (up to 40 vol.%) of accidental origin. It contains twisted trains composed of juvenile coarse ash (<1 mm) (<10 vol.%). Laminations pinch and swell laterally and are often truncated by overlying laminations. Cross-lamination is not uncommon. <5 mm-diameter, spherical/oval accretionary lapilli are displayed along discontinuous horizontal trains at some segments or else scattered randomly in the tuff. In some sections this facies may contain coarse accidental blocks (up to 40 cm) either forming impact sags or embedded in the tuff without deforming the tuff beds. Soft deformation is pervasive. The diffuse distributed juvenile fragments (up to coarse lapilli) may form incipient reverse-grading layers. The finer ash is composed of quartz, feldspar, and smaller amounts of clay; the coarser juvenile grains consists of basaltic glass (tachylite or sideromelane) with some, individual or clustered, olivine/pyroxene phenocrysts and abundant Ca-rich pyroxene microlites/microcrysts.

Interpretation: Intense soft deformation, poor sorting, accretionary lapilli, cross-lamination indicate the deposition of wet base surges that were transported in a low-energy, rapidly decelerating cloud. The presence of juvenile trains of variable thickness may suggest also traction carpet mode of transportation. (Sohn, 1997; Sohn and Chough; 1989; Chough and Sohn, 1990).

T4 (Figs. 5.5c, 5.6c). Poorly consolidated, diffusely stratified, light brown tuff sequences up to 0.5 m in thickness. It is poorly sorted and mainly composed of fine ash (~up to 40 vol.%) and medium ash (~ up to 30 vol.%) of accidental origin. It contains segments with concentration (30-40 vol.%) of diffusely distributed, inverse graded, juvenile coarse ash (<2 mm) which forms continuous, parallel/sub-parallel bands (up to 10 cm thick) with no distinct upper/lower boundaries. The bands thin upwards and the size of their juvenile fragments becomes finer. It also contains continuous, parallel/sub-parallel trains composed of juvenile, coarse ash (<1 mm) (<10 vol.%) randomly distributed. <5 mm-diameter, spherical/oval accretionary lapilli are displayed along discontinuous horizontal trains at some segments or else scattered randomly in the tuff. The finer ash is composed of quartz, feldspar, and smaller amounts of clay; the coarser juvenile grains consists of basaltic glass (tachylite or sideromelane) with some, individual or clustered, olivine/pyroxene phenocrysts and abundant Ca-rich pyroxene microlites/microcrysts

Interpretation: The presence of juvenile richer bands, accretionary lapilli, and poorly sorting point to the deposition of density stratified, wet, moderately diluted PDCs that were transported as a combination of low-turbulent suspended loads and traction carpets in a sustained fashion. The upwards thinning of juvenile richer bands may suggest progressively more suspended load mode of transport with the incorporation of finer and less abundant juvenile clasts. (Sohn, 1997; Sohn and Chough; 1989; Chough and Sohn, 1990; Dellino et al., 1990).

T5 (Figs. 5.5b,c; 5.6c,e). Moderately consolidated, poorly sorted, diffusely and/or crudely stratified tuff sequences up to 0.5 m in thickness. Composed of up to ~70 vol.% of juvenile clasts with grain sizes ranging from fine lapilli (4 mm) to more common coarse ash (usually 1 mm to 0.3 mm) embedded in a matrix composed of fine to medium-sized, light brown ash of accidental origin (up to 30 vol.%). Juvenile fragments are distributed across the sequence forming continuous parallel trains; up to ~3 cm-thick, continuous, parallel, diffuse bands; or else non-stratified, randomly scattered arrangements. Subtle

inverse grading is observed at times. Beds are not affected by impact structures. Accretionary lapilli were not observed, but some of the juvenile fragments are coated with a fine layer of accidental ash. The finer ash is composed of quartz, feldspar, and smaller amounts of clay; the coarser juvenile grains consists of basaltic glass (tachylite or sideromelane) with some, individual or clustered, olivine/pyroxene phenocrysts and abundant Ca-rich pyroxene microlites/microcrysts

Interpretation: Diffuse stratification, poorly sorting, ash-coated juvenile fragments suggest the deposition of moderately concentrated, low-energy, wet base surges that were transported mainly as bed loads/traction carpets in sustained manner. (Sohn, 1997; Sohn and Chough; 1989; Chough and Sohn, 1990).

T6 (*Figs 5.5d; 5.6d,h*). Moderately consolidated, poorly sorted tuff up to 1 m in thickness. Composed of a laterally continuous, parallel succession of segments composed of fine-to-medium sized, grey-light brown ash of accidental origin that alternate with sections that consist of medium-to-coarse, juvenile ash. The latter is arranged in trains, laminations, and thin beds or irregular thickness (from few mm to up to 3 cm). The accidental content is up to 60 vol.%. At intervals, the presence of dark layers becomes more dominant; however, no distinct layers boundaries are shown. The finer-grained segments contain moderate amounts of <5 mm-diameter, accretionary lapilli. The sequence is virtually devoid of lapillus and block size fragments either of lithic or juvenile origin Soft deformation is not intense. The finer ash is composed of quartz, feldspar, and smaller amounts of clay; the coarser juvenile grains consists of basaltic glass (tachylite or sideromelane) with some, individual or clustered, olivine/pyroxene phenocrysts and abundant Ca-rich pyroxene microlites/microcrysts

Interpretation: Accretionary lapilli, parallel bedding, juvenile-rich beds with diffuse boundaries indicate the deposition of density stratified, weak-turbulent, rapidly decelerating, wet base surges that were mainly transported as suspended loads and bed loads. (Sohn, 1997; Sohn and Chough; 1989; Chough and Sohn, 1990; Dellino et al., 1990)

T7 (*Figs. 5.5a,d,h*). Poorly consolidated, faintly laminated, vesicular, unaltered (light brown to cream) to heavily altered tuff sequences up to 1.5 m in thickness. It is poorly sorted and composed mainly of fine-to-medium ash of accidental origin up to 70 vol.%. It contains continuous, sub-parallel trains composed of juvenile coarse ash (<1 mm). Subtle low-angle, discontinuous cross lamination is present at intervals. The presence of <5 mm-diameter, spherical/oval accretionary lapilli is ubiquitous. The sequence is virtually devoid of lapillus and block size fragments either of lithic or juvenile origin Soft deformation is not intense. The finer ash is composed of quartz, feldspar, and smaller amounts of clay; the coarser juvenile grains consists of basaltic glass (tachylite or sideromelane) with some, individual or clustered, olivine/pyroxene phenocrysts and abundant Ca-rich pyroxene microlites/microcrysts

Interpretation: Accretionary lapilli, cross-lamination, juvenile-rich beds with diffuse boundaries indicate the deposition of density stratified, low-energy, rapidly decelerating, wet PDCs that were mainly transported as suspended loads and bed loads. (Sohn, 1997; Sohn and Chough; 1989; Chough and Sohn, 1990; Dellino et al., 1990)

Lapilli-tuff:

LT1 (Figs. 5.5c,d,e; 5.6a,b,d,f). Moderately consolidated tuff that forms beds that range from approximately 3 to 10 cm in thickness and form sub-parallel and/or slightly undulating, laterally continuous layers. The layers pinch and swell when encounter an obstacle. It is poorly sorted and composed of >80 vol.% of coarse ash to fine lapilli juvenile fragments. The beds are dominantly clast supported, ungraded, and normal or reverse graded, and may show scour surfaces of bed load structures. The poorly vesicular, sub-angular, juvenile fragments may be embedded in an incipient and irregularly widespread matrix of light coloured, fine-to-medium ash of accidental origin (<20 vol.%). Rare accidental/juvenile fragments bigger than fine lapillus size are present, as well as scarce <1 cm, accretionary/armoured lapilli. The finer ash is composed of quartz, feldspar, and smaller amounts of clay; the coarser juvenile grains consists of slightly to moderately palagonitized basaltic glass (tachylite or sideromelane) with some, individual or clustered, olivine/pyroxene phenocrysts and abundant Ca-rich pyroxene microlites/microcrysts.

Interpretation: The degree of consolidation, poorly sorting, pinch and swell, and variable grading may point to the deposition of a relatively high concentrated, wet PDCs transported dominantly in a traction carpet mode. These beds may have been part of a denser fraction of a PDC that became density segregated or decoupled. With distance, the flow was transformed into a granular fluid-based PDC. Grain addition of fall-out clasts into the already moving flow is not ruled out, but was probably never dominant. (Valentine, 1987, Fisher, 1995; Branney and Kokelaar, 2002; Vazquez and Ort, 2006)

LT2 (Figs. 5.5a,c; 5.6a,b,d,g). Moderately consolidated tuff beds that are laterally continuous, but notably vary in thickness (pinch and swell), exhibiting at times contorted and deformed beds. It is poorly sorted and composed of >80 vol.% of coarse to fine lapilli juvenile fragments. The beds are dominantly clast supported, ungraded, and normal or reverse graded. Intense soft deformation is evident and beds can be affected by impacts of blocks of accidental origin (up to 40 cm). Juvenile fragments are poorly vesicular and sub-angular and may be embedded in an incipient and irregularly widespread matrix of light coloured, fine-to-medium ash of accidental origin. Rare accretionary/armoured lapilli are present. The finer ash is composed of quartz, feldspar, and smaller amounts of clay; the coarser juvenile grains consists of slightly to moderately palagonitized basaltic glass (tachylite or sideromelane) with some, individual or clustered, olivine/pyroxene phenocrysts and abundant Ca-rich pyroxene microlites/microcrysts.

Interpretation: Intense soft deformation. The degree of consolidation, poorly sorting, and variable grading may point to the deposition of a relatively high concentrated, wet PDCs transported dominantly in a traction carpet mode and later deformed by impact fragments. These beds may have been part of a denser fraction of a PDC that became density segregated or decoupled. Grain addition of fall-out clasts into the already moving flow was probably more important than for LT1. (Valentine, 1987, Fisher, 1995; Branney and Kokelaar, 2002; Vazquez and Ort, 2006)

LT3 (Fig. 5.5b,e). Consolidated, massive-to-crude bedded tuff forming beds up to 0.5 m thick. It is poorly sorted and composed of >90 vol.% of coarse ash to fine lapilli juvenile fragments. The beds are dominantly clast supported, ungraded, and normal or reverse graded, and may show load structures at the base. The juvenile clasts are poorly to moderately vesicular, sub-angular, and slightly to moderately

palagonitized. It is possible to discern some fine, light coloured ash present as an incipient matrix and also irregularly distributed as subhorizontal, subparallel, and laterally continuous laminae (<1 cm thick). Rare accidental/juvenile fragments bigger than fine lapillus size are present, as well as scarce <1 cm, accretionary/armoured lapilli. The finer ash is composed of quartz, feldspar, and smaller amounts of clay; the coarser juvenile grains consists of slightly to moderately palagonitized basaltic glass (tachylite or sideromelane) with some, individual or clustered, olivine/pyroxene phenocrysts and abundant Ca-rich pyroxene microlites/microcrysts.

Interpretation: The high degree of consolidation, palagonitization, and juvenile clast morphology may suggest the deposition of a high concentrated, wet, non-turbulent PDC probably emplaced more like a Surtseyan tephra jet transported as a grain flow. The transformation into lithofacies T5 downhill may indicate that it was transformed into a more density stratified-like, diluted PDCs. The entrainment of further fall-out fragments is not discarded, but seems not to be the dominant process. (Kokelaar, ,1983; Sohn and Chough, 1992; Sohn and Chough, 1993).

2. LITHOSTRATIGRAPHIC UNITS

Stratigraphic and sedimentary criteria to describe the units are provided in chapter 5. The lithofacies included in the descriptions of units are described in the text above or briefly on Table 5.3. The condensed information of these units is presented in Table 3 in chapter 5. All referred figures are displayed in chapter 5.

UNIT 1

U1 is defined within the lowest part of the tuff-ring basal deposits (Figs. 5.2 and 5.5c,e) and overlies pale brown muds and peaty paleosols with a sharp irregular contact (seen around sites M3 and M5). At site M3, the brownish-grey unit is ~1.5 m thick and characterized by crudely stratified, parallel-to-subparallel bedded, poorly consolidated tuff (lithofacies T1) and thin beds (<8 cm) of dominantly clast-supported, poorly-to-moderately consolidated, poorly sorted lapilli tuff (lithofacies LT1). Occasional rounded-subrounded <15 cm-diameter country rock ballistic clasts form impact structures, or are embedded in the tuff. They are formed by undeformed aggregates of Pliocene-Pleistocene (Kaawa and Tauranga Fm) sediments. The impact bedding sags are <10 cm deep, plastically deformed, and slightly asymmetric, with impact angles approximately ESE-WNW orientated. The tuff comprises >90% by volume of medium ash, that is >80% by volume of lithic. Randomly throughout the unit, horizontal trains of juvenile subangular, poorly-to-moderately vesicular, medium-lapilli occur. Variably abundant, but ubiquitous, <5 mm diameter, spherical and oval shaped accretionary lapilli are contained in the fine-grained beds throughout this unit, increasing in abundance upwards. At site M5, U1 is ~0.5 m thick (Fig. 5.5e), showing similar contacts with underlying peat/sediment, where lithofacies T1 becomes distinctively unbedded, massive, and composed of >95% in vol. of medium to fine ash.

Interpretation

The onset of the phreatomagmatic activity is represented by fine tuff (T1) dominantly comprising accidental feldspar and quartz grains derived from the Kaawa, Tauranga, and Waitemata lithologies (see section 2 in the main text for general descriptions of these Formations). The absence of massive,

country rock-rich, block or lapilli-bearing breccias characteristic of vent-clearing phases (e.g., Sohn and Chough, 1989) is due to the locus of initial explosions within shallow saturated and unconsolidated sediments. However, the lower tephra ring deposits do not necessarily represent the early ejecta from the maar (Valentine, 2012). These early explosions generated pyroclastic density currents (PDCs) containing ash-dominant particles. The PDCs were wet, either due to condensation of steam and/or original sediment pore water. Ash particles were cohesive, forming accretionary lapilli. The base surges rapidly decelerated and the lithofacies features represent weakly turbulent to laminar flow regimes (c.f., Zimanowski and Wohletz, 2000). Juvenile-clast trains in medial sites (site M3) with no distinct boundary layers indicate unsteady pulsatory base surges with variable grain size supply (c.f., Sohn, 1997; Sulpizio et al., 2008), and high rates of deposition. At this point, particles within the base surges travelled mostly in a tractional/saltational regime in which collisional mechanisms were practically absent (similar to fully dilute PDCs of Branney and Kokelaar, 2002). In distal locations (site M5, Fig. 5.5e), the base surges had degraded into fine-ash dominant, low-energy turbulent clouds, forming massive deposits mainly by particle settling (e.g., Wohletz and Sheridan, 1979; Sulpizio and Dellino, 2008).

UNIT 2

Along a segment from sites M3 to M4 (Fig. 5.2), U2 consists of a characteristic alternation of <10cm beds of coarse-ash to fine lapilli-sized, poorly-to-moderately vesicular, subangular, juvenile pyroclasts (lithofacies LT1), with inter-beds of pale brown-coloured, lithic dominated ash (lithofacies T2). At M1, U2 shows variable thickness (up to ~0.5 m), is faulted (Fig. 5.5a), and constituted by lithofacies LT2 and T2 (described above). At site M3, the lowermost LT1 bed shows a sharp contact with the underlying U1. At the contact, there are scour surfaces, load structures, impact structures from coarse lapilli/blocks that include both rounded, accidental lithics and poorly-vesicular, juvenile clasts (Figs. 5.5c and 5.6a,b). LT1 beds become thinner, finer grained, and have more diffuse contacts upwards (Fig. 5.6a,b). The distal sites, between M4 and M5 are characterized by a ≤0.5 m-thick U2, with 0.5 m-amplitude undulating layers of alternating lithofacies LT1 and T2 (Figs. 5.5e and 5.6d). At distal locations, hollow casts occur within U2 (up to 30 cm-thick across) from logs that have rotted out of the tuff virtually at sea level (Fig. 5.6d). Poorly-to-moderately abundant, <5 mm, spherical/oval accretionary lapilli/armoured lapilli occur in the finer-grained layers.

Interpretation

The presence of a coupled lower coarser-grained-rich bed (LT1) overlain by a finer-grained-laden layer (T2) suggests that U2 was formed by a series of density stratified PDCs (e.g. Valentine 1987) generated from both the collapse of small eruptive clouds as well as tephra jets (secondary and primary surges, respectively of Wohletz, 1998). These yielded concentrated and mostly wet flows. They were homogeneous very close to the vent, but were soon partitioned into two layers. The rather erosive basal part was concentrated in juvenile particles (lithofacies LT1) (e.g., Vazquez and Ort, 2006) and transported as a frictional/traction carpet (similar to the granular fluid-based PDCs of Branney and Kokelaar, 2002). By comparison, the less dense overlying portion was finer-grained and transported particles in a saltation-dominated bed load regime at its base, passing upward into a turbulent suspended load (lithofacies T2). Each PDC produced a deposit couplet (c.f., Vazquez and Ort, 2006). Following waning explosions produced pulsating successive PDCs. A fining upwards of juvenile

particles in U2 may indicate increasing efficiency of phreatomagmatic fragmentation (c.f., Sheridan and Wohletz, 1983), and/or possibly fall-back and re-fragmentation of recycled clasts (e.g., Houghton and Smith, 1993). Outward to medial distances the base surges were dominantly transported in the saltating to turbulent regime, producing more diffuse beds, but traction carpet mode of transport was still in effect. With distance from the vent, the pyroclastic currents became wetter and topographically controlled..

UNIT 3

In the most proximal location (M1, Fig. 5.5a) this unit is difficult to distinguish due to inner rim wall subsidence/faulting and weathering. With an average thickness of 0.7 m, U3 is best represented in the medial sites (M3) by layers of massive to crudely stratified, fine-to-medium ash tuff (with continuous subparallel trains) (lithofacies T3) and moderately consolidated, moderately sorted lapilli tuff (lithofacies LT2) (Fig. 5.5c). The lower and upper unit contacts and those between lithofacies are gradational. Accidental blocks (up to 25 cm in diameter) are mainly contained in the mid portions, plastically deforming the LT2 bed, the underlying T3, and at least in one location affecting slightly the uppermost part of the underlying U2 (Fig. 5.5c). >90 vol.% of sub-rounded to rounded blocks are composed of fragments of the Waitemata Group. Aggregates of Pliocene-Pleistocene sediments, which do not show plastic deformation and internal structures are also present (<10 vol.% of accidental blocks). Towards M4, the contact down to U2 is distinct but still gradational (Fig. 5.5d). Lithofacies T6 (moderately consolidated tuff composed of an alternation of thin layers of accidental-origin ash and relatively coarser, juvenile ash) and LT1 comprise this unit (Fig. 5.5d). Ballistic impacts are more subdued in distal outcrops. The thickness of U3 is roughly ~0.5 to ~0.7 m and varies little from proximal to distal locations (Fig. 5.2), although at the latter it lies at or near the sea level (Fig. 5.2). Accretionary lapilli (<1 cm diameter) occur scattered throughout.

Interpretation

This phase starts with lithofacies T3 deposits (sites M1 and M3, Fig. 5.5a,c), indicating PDCs with an unsteady and pulsatory behaviour, with multiple terminating trails of coarser juvenile fragments (c.f., Sulpizio and Dellino, 2008). This was followed by deposition of LT2 along with the first appearance of ballistic blocks derived sub-lithified Waitemata Group lithologies (Fig. 5.5c and 5.6a,b), which indicates a deepening locus of explosions and/or shifting of vent. Finally, a renewed series of unsteady and pulsating base surges (lithofacies T3) occurred. In medial to distal sites (at site M4, Figs. 5.5d and 5.6d), particles are transported mainly within bed loads. Towards the top of U3, coarse juvenile fragments were emplaced in a massive lapilli tuff, but very rare accidental blocks, possibly indicating that explosions did not progress further vertically or laterally into the Waitemata Group.

UNIT 4

At site M1 (proximal site), the tuff is weathered and comprises both undulating/deformed and undeformed beds of lithofacies T3 (Fig. 5.5a). At M2, the upper boundary with U5 is sharp and horizontal (Fig. 5.5b) and constituted of lithofacies T1. Unit 4 at site M3 stands at ~3 m above mean sea level (Fig. 5.2), is ~0.5 m-thick, and composed of poorly consolidated and moderately stratified ash tuff that contains continuously parallel and diffuse concentrations of trains (bands) composed of fine, juvenile lapilli (lithofacies T4) (Figs. 5.5c and 5.6c). At least at M2 to M4, the sequence is devoid of

coarse accidental clasts and its upper and lower boundaries are gradational. The rhythmically bedded T4 lithofacies become the diffusely stratified T6 lithofacies (moderately consolidated tuff composed of an alternation of thin layers of accidental-origin ash and relatively coarser, juvenile ash) at site M4 (Figs. 5.5d and 5.6d). Juvenile fragments reduce in size. U4 reduces in thickness by at least 30% from medial to distal sites. Sites M2 and M4 contain <5 mm-diameter, accretionary lapilli in the lithofacies T1 and T6.

Interpretation

The eruption proceeded without interruption as suggested from the gradational contact from U3 to U4. Lithofacies T4 indicates a rhythmic sequence of PDCs with progressively lower contents of finer-grained juvenile fragments. Juvenile-rich bands and trails are fine-grained and show no distinct boundary layers, which indicates that base surges were generated by the recurrent collapse of low eruption columns formed by semi-continuous eruptions (c.f. Dellino et al., 1990). Deposition in medial locations was from moderately-dilute, weakly-turbulent clouds, which rapidly deflated, reduced in turbulence and particle load, depositing lithofacies T6 (Fig. 5.6a). Soft-sediment deformation is more evident in proximal locations (Fig. 5.5a), corresponding to inner rim wall subsidence. The absence of Waitemata Group block/lapilli-sized accidentals may suggest that the deposited material did not originate from freshly excavated Waitemata host rock by deepening of the explosion locus or a shifting in the vent, but rather from shallow seated explosions (Valentine and White, 2012).

UNIT 5

This unit cannot be recognised in its entirety. At site M2, U5 comprises a sequence of moderately to poorly consolidated, crudely bedded, variably clast supported, juvenile lapilli tuff (lithofacies LT3 and ash tuff (lithofacies T2 and T4). The ~1 m-thick sequence, containing >5 mm accretionary lapilli, has continuous plane-parallel bedding with sharp contacts onto underlying ash-rich U4 that are deformed by load structures (Fig. 5.5b). Within the unit, contacts are sharpest between lithofacies T2 and LT3, but gradational between lithofacies LT3 and T4, (Fig 5.5b). Blocks and bombs are rare and small, bordering on coarse-lapilli-sized clasts that form roughly asymmetric shallow bedding sags (~5 cm) with low impact angles. At M3, U5 thins to ~0.7 m. Its lower and upper coarse-grained segments become two diffuse bedded succession (with no boundary layers) containing juvenile fragments interbedded with accidental-origin ash (lithofacies T5). At site M4, lower and upper unit boundaries are ill-defined with bounding units being characterized by similar plane-parallel bedded, diffusely stratified tuff sequences (lithofacies T6). At site M4 many of the lithofacies have merged and U5 is represented by <0.5 m of laminae of variable juvenile-content (lithofacies T6) (Figs. 5.5d and 5.6d). At distal sites, T6 lithofacies contain accretionary lapilli.

Interpretation

A sharp contact to the base of this unit, lithofacies LT5 shows that the eruption shifted suddenly to a phase of production of coarser and more common juvenile fragments, either due to a reduction of external water interaction (it is possible that it represents a very shallow explosion, where water was restricted), or an increase in magma ascent rate (c.f., Houghton et al., 1999). Deposition of this phase from PDCs was mainly via traction-carpet collisional regimes close to the vent. The sequences containing higher lithic content (lithofacies T2 and T4 -Fig. 5.5b) could possibly indicate inner vent-

wall/sediment slumping into the explosion locus (c.f., Houghton and Smith, 1993) causing transient variations in degrees of interaction of the magma with external water and/or changes in magma ascent rates (Houghton et al., 1999). The final stages of this phase produced again juvenile-rich beds (lithofacies LT5), similar to its onset. An outstanding feature of U5 is the progressive transformation of sediment character from proximal to distal sites (Figs. 5.5b,c,d). The coarse, juvenile-rich layers (Fig. 5.5b) become gradually more distinctly stratified, with diffuse boundaries and composed of finer-grained juvenile fragments, which are distributed scarcely (Figs. 5.5c,d). U5 at site M3 (Fig. 6c) may have been deposited following stepwise aggradations (Sulpizio and Dellino, 2008) of a PDC (or PDCs) dominantly transported in a collisional regime. Although the number of layers deposited by the passage of a single base surge is to an extent uncertain (Dellino et al., 1990), the polymodal clast distribution and the lack of erosional breaks in a deposit could indicate closely-timed explosions (Dellino et al., 1990), which generated numerous PDCs that in turn may segregated into different pulses that travel independently from each other (Sulpizio and Dellino, 2008). In travelling away from the vent, the PDCs became less concentrated and transported in a combination of saltation/traction mode producing mainly plane parallel-bedded deposits (as described in Valentine, 1987) (Figs. 5.5d and 5.6d).

UNIT 6

U6 is the uppermost tuff-ring sequence, and is commonly eroded and weathered (Fig 5.2). There are at least three lithofacies preserved T5, T6, and T7 (accretionary lapilli-rich, vesicular, fine-grained, lithic ash tuff. At M1 the deposits are ~1.5 m thick and lithofacies T7 dominates (Fig. 5.5a). Beds are parallel, continuous and form a gentle syncline-like structure, and are not affected by faulting as in the lowermost units at this site. At site M2, U6 is <1 m thick and comprises lithofacies T7 and T5 (Fig. 5.5b). At medial locations around site M3, U6 is usually <1 m (Fig. 5.5c). At M4, however, the unit thickens again to ~1.5 m and comprises continuous, plane-parallel beds alternating between lithofacies T7 and T5 (Figs. 5.5d and 5.6c). The pale/cream tuff is dominantly finer than coarse ash (with rare fine lapilli), contains sub-mm, irregular-to-rounded vesicles and ≤ 5 mm-diameter, spherical/oval accretionary and armoured lapilli.

Interpretation

Along the cliff, it has an irregular thickness ranging from mostly <1m, with lenses up to 2 m, which may reflect its deposition in separate lobes rather than a continuous sheet. U6 is characterized by lithofacies T7 and T6 (Fig. 5.5a,d), which shows a regular pattern of deposition from PDCs. Although soft sediment deformation of beds is subdued (due to a paucity of fragments larger than coarse ash), the presence of abundant accretionary lapilli and the vesicularity of tuff indicates its depositing currents were wet, with condensed water (e.g. Dellino et al., 1990). The level of explosive fragmentation (e.g., the depth of the explosive eruption locus) probably remained shallow-seated as indicated from the widespread presence of fine-grained material possible sourced from an already comminuted fragmented host rock redeposited within the upper diatreme (Valentine and White, 2012). The thicker U6 accumulations at the inner rim and in the distal location could reflect either the topographic barrier of the inner rim (c.f., Sulpizio and Dellino, 2008), or the lofting and subsequent grounding of the currents as they accelerated over the rim (Sohn, 1996). In general, the succession exhibits regular deposition patterns that suggest stabilization of the vent with explosions remaining in the water-saturated poorly unconsolidated sediments.

Appendix C. Chemical analyses

C.1 Chemical analyses Maungataketake

C.1.1 Whole-rock analyses

Samples from Maungataketake Volcano analyzed for major and trace elements were collected from the ejecta ring (3 samples) and the central scoria/lava cone (16 samples) to represent the range of materials erupted from the volcano; these data are presented in Table A.1. The samples are juvenile bombs from within tuff sections, scoriaceous blocks and lava. Rock fragments were crushed in a tungsten carbide ring grinder to <200 μ mesh. Major elements and some trace elements were analyzed by XRF on fused glass discs made using Lithium Borate Spectrachem 12-22 flux, using a Siemens SRS3000 sequential X-ray spectrometer with a Rh tube at the University of Auckland. Minor trace elements were measured on a Laser Ablation Inductively Coupled Mass Spectrometer (LA-ICP-MS) at the Australian National University using stacks of XRF discs following the procedure of Eggins et al (1998). NIST 612 was run every 15 samples and used for calibration, and the silica content obtained by XRF used in data reduction. BCR-2G was used as an external standard with every analytical session and 28 international standards provided a further check on the method. BCR-2 data (n=143) is <15% 2SD, and accuracy <10% for all elements except Cu, Y, Zr, Tb and Hf which are <17% and Cr which is <26%. XRF data is reported for Cr, Ni and Zr.

C.1.2 Glass analyses

10 juvenile grains were selected (from thin sections) for microprobe analyses. These grains represent 5 samples taken from different sites (see Fig. 5.2 in main text for location of units, U, and sites, M): sample 26 (from middle U3 at site M1) (2 grains), sample 28 (from upper U3 at site M1) (3 grains), sample 31 (from middle U5 at site M2)(2 grains), sample 40 (from lower U6 at site M5)(2 grains), and sample 41 (from upper U6 at site M5)(1 grain). 6 spot measurements per grain were run on different glass sites. An average glass composition of each grain is shown in Table A.2. These compositions have been plotted and are shown in Fig. 5c,d. Olivine phenocrysts (not shown) and Pyroxene microlites/microcrysts were also analyzed and are represented in Fig. 5e. 15 pyroxene crystals were analysed from the same 5 samples mentioned above.

The samples were analysed by a Jeol JXA-8900R electron microprobe at the Laboratorio Universitario de Petrología (LUPI), Instituto de Geofísica, UNAM, México City. Measuring conditions were a beam current of 10 nA, an accelerating potential of 20 kV, and a beam diameter of 15 μ m for glass and 1-5 μ m for crystal analyses. During analyses, Na and K were analysed using 10 s counting times, whereas a 40 s counting-time was used for other elements.

Sample	26a	26b	28a	28b	28c	31a	31b	40a	40b	41
SiO ₂	44.85	46.16	41.92	46.74	46.84	42.88	43.03	45.16	46.01	44.61
TiO ₂	3.32	3.30	3.27	3.04	3.16	3.41	3.43	3.39	3.13	3.44
Al ₂ O ₃	15.75	15.90	15.56	16.44	16.23	15.48	15.48	15.49	16.11	15.58
FeO	13.29	13.20	12.84	12.52	12.74	13.19	13.27	13.10	12.94	13.20
MgO	4.05	4.10	4.01	3.78	4.06	4.21	4.22	4.20	3.85	4.33
CaO	11.31	11.35	11.25	10.77	11.08	11.69	11.67	11.61	10.95	11.73
Na ₂ O	5.16	5.04	4.91	5.12	4.95	3.88	3.86	4.04	4.20	4.11
K ₂ O	1.93	1.93	1.86	1.99	1.93	1.92	1.87	1.89	1.89	1.89
Total	99.67	100.98	95.63	100.40	100.98	96.67	96.82	98.88	99.09	98.89
Mg#	35.22	35.63	35.77	36.21	35.01	36.28	36.20	36.38	35.22	36.90

Table C.2 Average glass composition of selected juvenile clasts from Maungataketake volcano. Mg# calculated as mole percent Mg/Mg+Fe x100. Each sample number (see Appendix 2 for sample details) can be represented by one up to three single grains which are indicated by letters (*a,b,c*).

C.2 Glass analyses of North Head

Groundmass glass compositions were analysed at the University of Auckland with a JEOL JXA-840 electron microprobe microanalyser (EPMA) interfaced with a Princeton Gamma Tech Prism 2000 Si (Li) EDS X-ray detector at an accelerating voltage of 15 kV, a beam current of 800 pA and a total count time of 100 s. 17 juvenile sideromelane grains were selected (representing different levels from PH1, PH3, and PH4); up to three spots were analysed on each grain. The characteristics and location of each unit PH are explained in Chapter 7.

Sample	PH1-1a	PH1-1b	PH1-1c	PH1-2a	PH1-2b	PH1-2c	PH1-3a	PH1-3b	PH1-3c	PH1-4a	PH1-4b	PH1-5a	PH1-5b	PH1-6a	PH1-6b	PH1-7a	PH1-7b	PH1-7c	PH3-1a	PH3-1b	PH3-1c
SiO ₂	46.8	46.5	46.9	46.6	46.4	46.6	46.8	46.6	46.4	47.3	47.0	47.1	46.9	46.8	47.0	46.4	46.1	46.9	46.7	46.8	46.4
TiO ₂	2.9	3.0	2.9	3.2	3.1	2.7	2.6	2.7	2.6	2.8	2.7	2.6	2.8	2.6	2.7	2.5	2.5	2.6	2.7	2.7	2.9
Al ₂ O ₃	17.1	16.7	17.0	16.7	17.1	16.9	17.3	17.1	17.1	17.1	16.9	17.1	17.1	17.2	17.1	17.0	16.8	16.7	17.1	17.1	16.9
FeO	10.6	10.8	10.9	10.6	10.6	10.3	10.5	10.4	10.6	10.2	10.5	10.3	10.4	9.8	10.4	10.0	10.1	10.1	10.5	10.2	10.4
MnO	0.2	0.1	0.3	0.2	0.3	0.3	0.2	0.2	0.3	0.2	0.1	0.2	0.1	0.2	0.3	0.2	0.1	0.2	0.2	0.1	0.2
MgO	3.2	3.3	3.2	3.3	3.4	3.0	3.1	3.1	2.9	3.2	3.1	3.4	3.4	3.3	3.2	3.0	3.1	3.3	3.1	3.1	3.2
CaO	8.4	8.3	8.5	8.9	8.7	8.3	7.9	7.9	7.9	8.1	8.0	8.3	8.2	7.7	7.8	7.8	7.8	8.0	8.0	7.9	8.0
Na ₂ O	4.9	5.2	5.3	4.7	5.1	5.3	6.0	6.1	5.6	5.8	5.4	5.6	5.8	6.0	5.7	5.4	5.4	5.4	5.2	5.4	5.5
K ₂ O	2.9	2.8	2.9	2.7	2.7	3.0	3.0	2.9	2.9	3.0	2.8	3.0	3.0	2.8	3.0	2.9	2.9	2.9	2.9	2.9	2.9
P ₂ O ₅	1.7	1.2	1.4	1.5	1.5	1.7	1.6	1.5	1.6	1.8	1.6	1.7	1.7	1.8	1.6	1.8	1.7	1.5	1.7	1.7	1.5
SO ₃	0.26	0.33	0.15	0.12	0.26	0.17	0.23	0.26	0.25	0.26	0.26	0.25	0.1	0.3	0.17	0.11	0.21	0.2	0.22	0.14	0.14
Cl	0.11	0.11	0.09	0.1	0.05	0.05	0	0.11	0.05	0.1	0.05	0.1	0.08	0.11	0.12	0.11	0.09	0.06	0.08	0.05	0.08
Cr ₂ O ₃	<0.11	0.05	<0.03	0.09	0	<0.03	0.1	<0.05	0.08	0.01	<0.01	<0.06	0.11	<0.01	0.01	0.05	0.05	0.19	0.09	0.04	<0.03
NiO	0.03	-0.04	<0.05	<0.09	0.02	0.02	0.08	<0.2	0.21	<0.01	0.08	<0.19	0.07	0.17	<0.03	0.23	<0.01	0.02	0.08	<0.09	0.02
Total	99.12	98.42	99.4	98.63	99.08	98.27	99.2	98.57	98.41	99.73	98.54	99.54	99.63	98.65	99.12	97.5	96.68	98.08	98.49	98.04	98.06
Sample	PH3-2a	PH3-2b	PH3-3a	PH3-3b	PH3-3c	PH3-4a	PH3-4b	PH3-5a	PH3-5b	PH3-6a	PH3-6b	PH3-7a	PH3-7b	PH3-7c	PH4-1a	PH4-1b	PH4-1c	PH4-2a	PH4-2b	PH4-3a	PH4-3b
SiO ₂	46.6	46.4	46.6	46.6	46.7	46.8	46.6	47.6	46.5	47.0	47.0	46.1	46.8	46.6	46.6	46.4	46.5	46.6	46.5	46.9	46.8
TiO ₂	2.8	2.9	2.6	2.8	2.8	2.7	2.7	2.7	2.8	2.6	2.5	2.6	2.9	2.9	2.7	2.7	2.9	2.9	2.9	2.8	2.7
Al ₂ O ₃	17.1	16.9	17.0	17.0	17.1	16.8	17.1	17.2	17.2	17.2	17.1	16.8	16.7	16.6	16.8	16.8	16.6	16.9	16.7	16.8	16.8
FeO	10.0	10.0	10.3	10.2	10.2	10.5	10.6	10.4	10.3	10.0	10.0	10.5	10.5	10.5	10.2	10.5	10.5	10.3	10.3	10.4	10.5
MnO	0.2	0.1	0.2	0.2	0.2	0.2	0.1	0.3	0.3	0.3	0.1	0.2	0.1	0.3	0.1	0.1	0.2	0.2	0.3	0.2	0.2
MgO	3.1	3.0	3.2	3.0	3.2	3.3	3.4	3.1	3.2	3.2	3.1	3.2	3.3	3.3	3.2	3.2	3.3	3.2	3.3	3.3	3.2
CaO	8.0	7.9	8.0	8.1	8.0	8.0	8.1	7.9	7.8	7.8	7.5	7.8	8.3	8.1	8.2	7.9	8.3	8.2	8.3	8.2	7.9
Na ₂ O	6.1	5.8	5.6	5.3	5.3	5.4	5.4	5.4	5.9	5.5	5.6	4.1	5.5	5.5	5.6	5.8	5.6	5.1	5.1	5.4	5.5
K ₂ O	2.8	2.8	2.9	2.9	2.9	2.8	2.9	2.9	3.0	2.9	2.9	2.7	2.8	2.8	2.9	2.8	2.8	2.9	2.8	2.9	2.9
P ₂ O ₅	1.7	1.5	1.7	1.7	1.6	1.8	1.6	1.7	1.7	1.6	1.6	1.5	1.5	1.5	1.7	1.5	1.6	1.6	1.6	1.6	1.5
SO ₃	0.1	0.2	0.3	0.2	0.2	0.3	0.2	0.3	0.2	0.2	0.1	0.2	0.1	0.3	0.2	0.1	0.1	0.1	0.2	0.3	0.2
Cl	0.1	0.1	0.1	0.1	0.1	0.1	0.1	0.1	0.1	0.1	0.1	0.1	0.1	0.1	0.1	0.1	0.1	0.1	0.1	0.1	0.1
Cr ₂ O ₃	0	0.08	<0.02	0.03	<0.05	0	0.03	0.04	0.17	0.06	0.1	<0.08	0.13	<0.02	0.15	0.04	0.05	<0.07	<0.13	<0.08	0.16
NiO	<0.01	<0.27	<0.1	0	<0.01	<0.02	0	<0.12	0.21	<0.19	0.04	<0.03	0.07	0.02	0.18	<0.08	0.01	<0.05	<0.05	0.02	0.09
Total	98.63	97.44	98.38	98.03	98.09	98.79	98.83	99.4	99.36	98.2	97.68	95.72	98.73	98.4	98.64	97.99	98.27	98.03	97.79	98.47	98.5

Table C.3. Glass compositions of 17 selected sideromelane clasts from North Head volcano. PH1-3-4 indicates the phreatomagmatic subunit where samples were collected. Samples come from varied stratigraphic positions within the units. The letters a, b, and c refer to the different spots analysed within the same clast.

Appendix D.1 Motukorea stratigraphic logs, grain size distribution and juvenile/lithic content of selected samples.

D.1.1 Motukorea stratigraphic logs

This part of the appendix first presents the total of logs corresponding to Motukorea volcano (Figs. D.1.2 to D.1.7). There are 3 extra logs included (SS1, SS2, and SS3). The logs showed in chapter 6 (S1, S2a, S2b, S3) are also included. See Table 6.2 in chapter 6 and Appendix D-2 for description of lithofacies included in logs and pictures.

Fig. D.1.1 shows an aerial photograph of Motukorea volcano. The exposed tephra ring deposits are clearly seen on the eastern-southern side of the island. The horizontal/vertical scale is approximate. Alongside the 4 sites described in chapter 6, other 3 sites are included (SS1, SS2, and SS3).

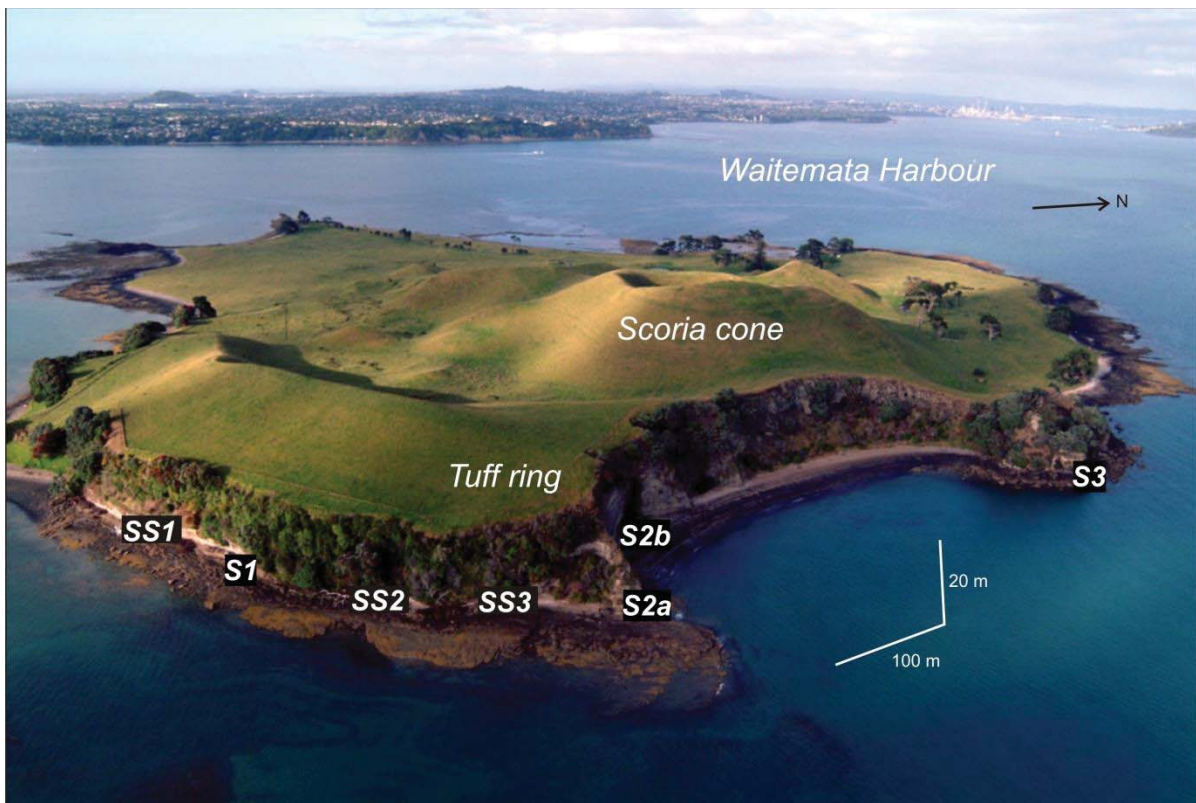


Fig. D.1.1 Location of complete studied sites.

The stratigraphic logs are presented starting from SS1 to S3. Except for exposures at site S2b (whose exposure base is at the back beach level) all other exposures' bases intersect a wave-cut platform that marks approximately the highest tide sea level in the area. The boxes, at the left of logs, containing the grain size and juvenile content are not to scale and do not represent stratigraphic columns. See Table 6.2 in chapter 6 and **Appendix D.2** for description of lithofacies

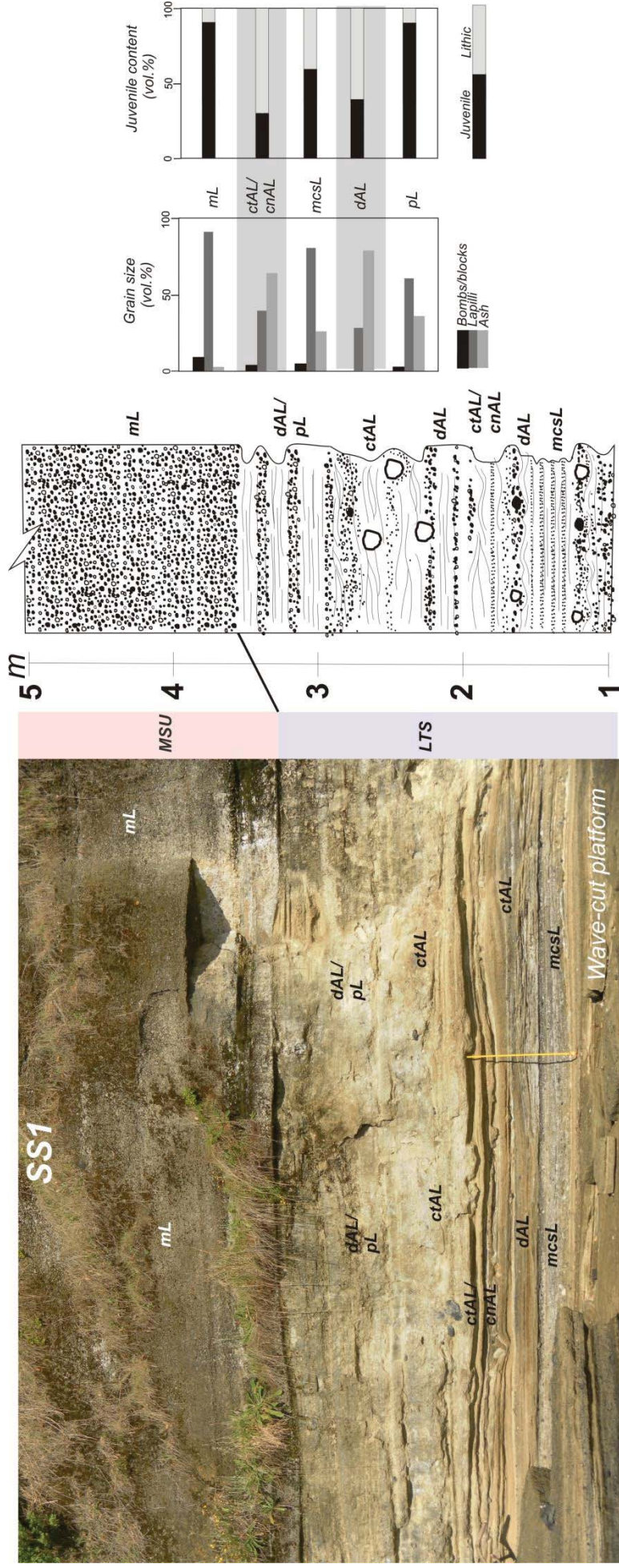


Fig. D.1.2 Site SS1. Base of sequence intersects a wave-cut platform that marks approximately the highest tide sea level in the area. Thickness of log (in metres) corresponds to thickness of sequence in photograph.

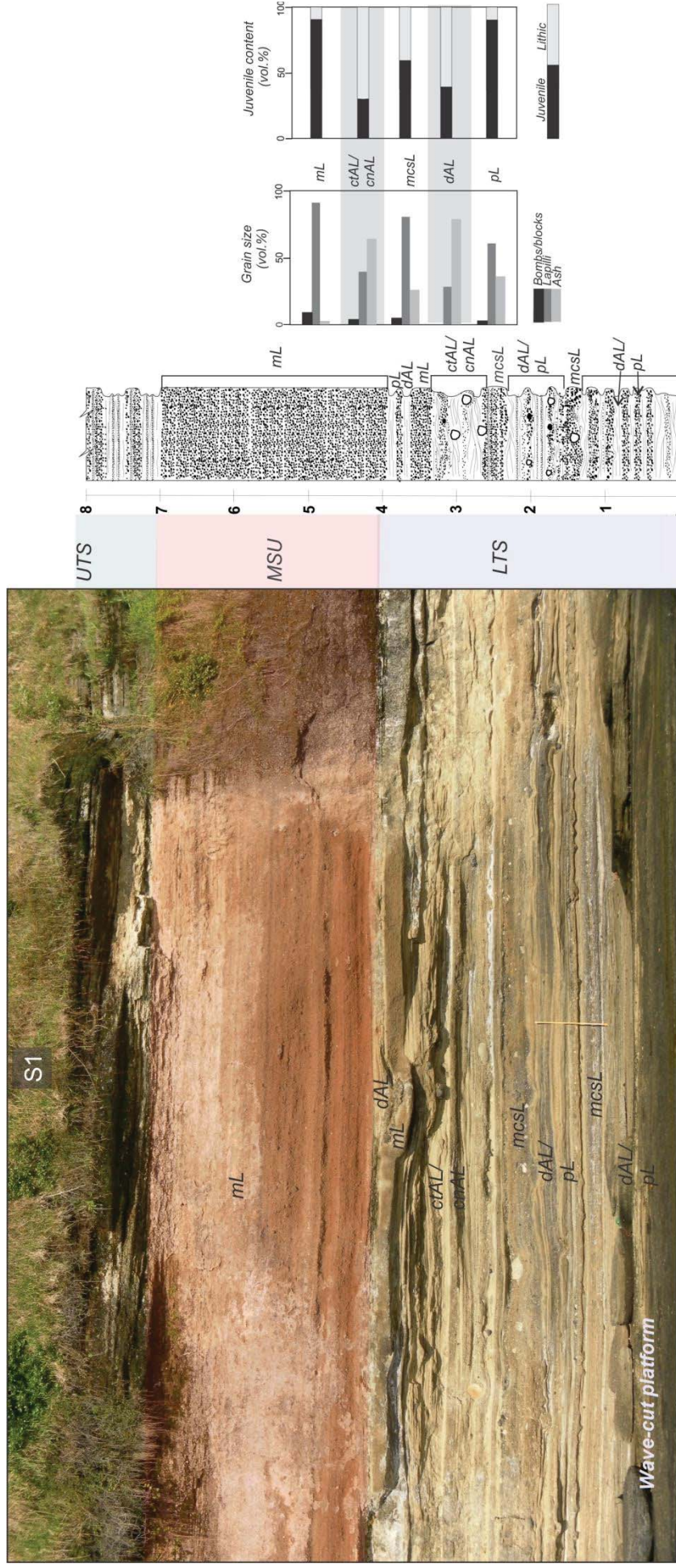


Fig. D.1.3 Site S1. Base of sequence intersects a wave-cut platform that marks approximately the highest tide sea level in the area. Thickness of log (in metres) corresponds to thickness of sequence in photograph.

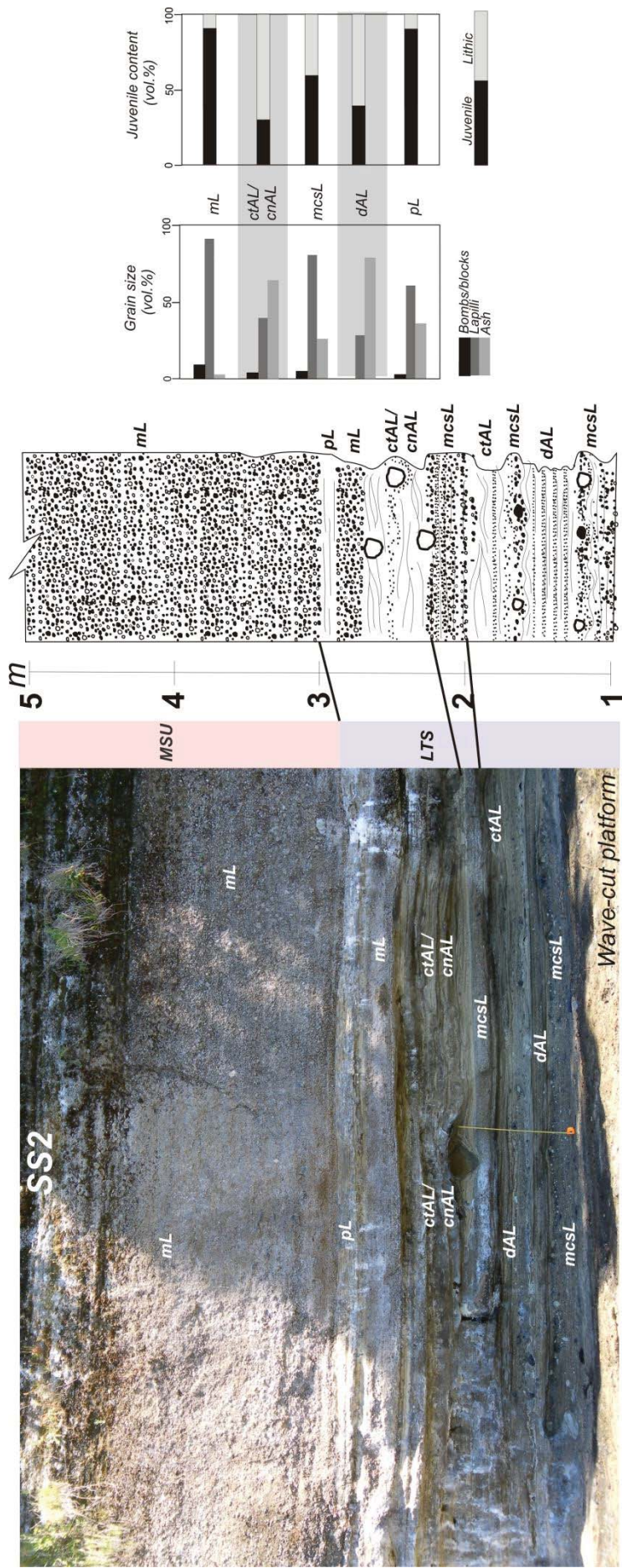


Fig. D.1.4 Site SS2. Base of sequence intersects a wave-cut platform that marks approximately the highest tide sea level in the area. Thickness of log (in metres) corresponds to thickness of sequence in photograph.

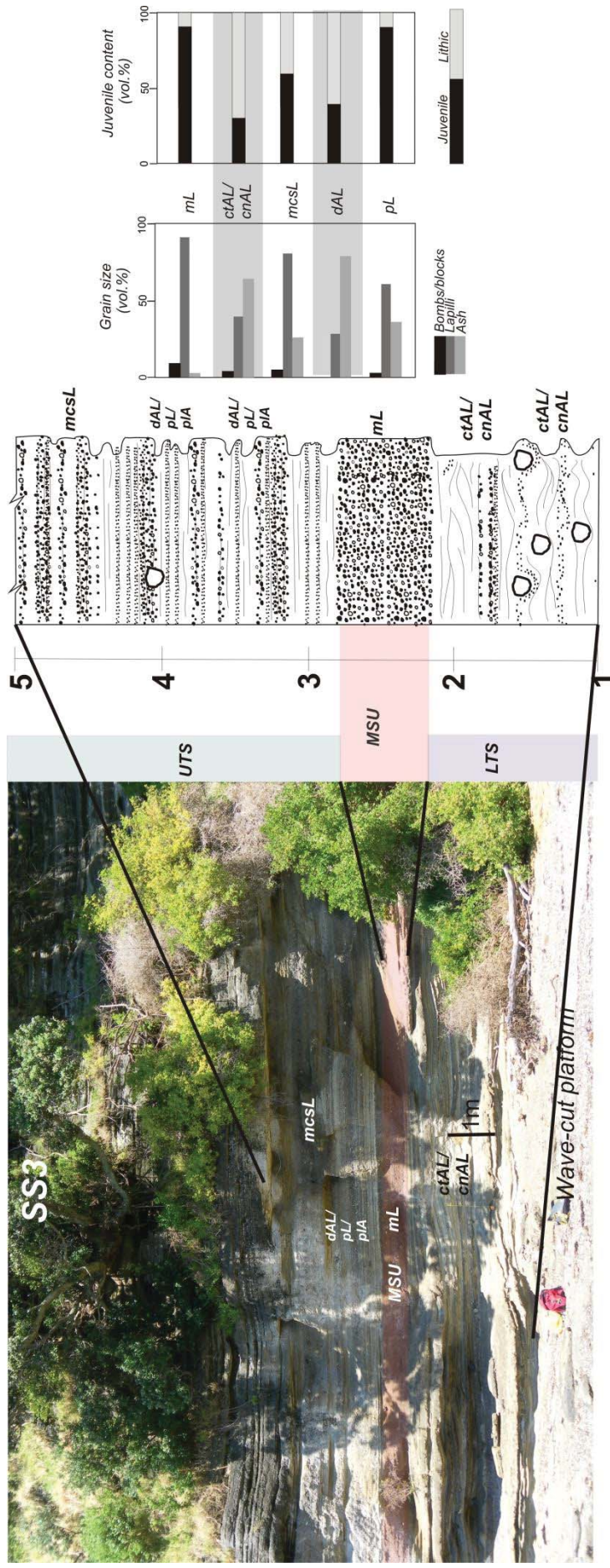


Fig. D.1.5 Site SS3. Base of sequence intersects a wave-cut platform that marks approximately the highest tide sea level in the area. Thickness of log (in metres) does not correspond to thickness of sequence in photograph (see scale bar in photograph).

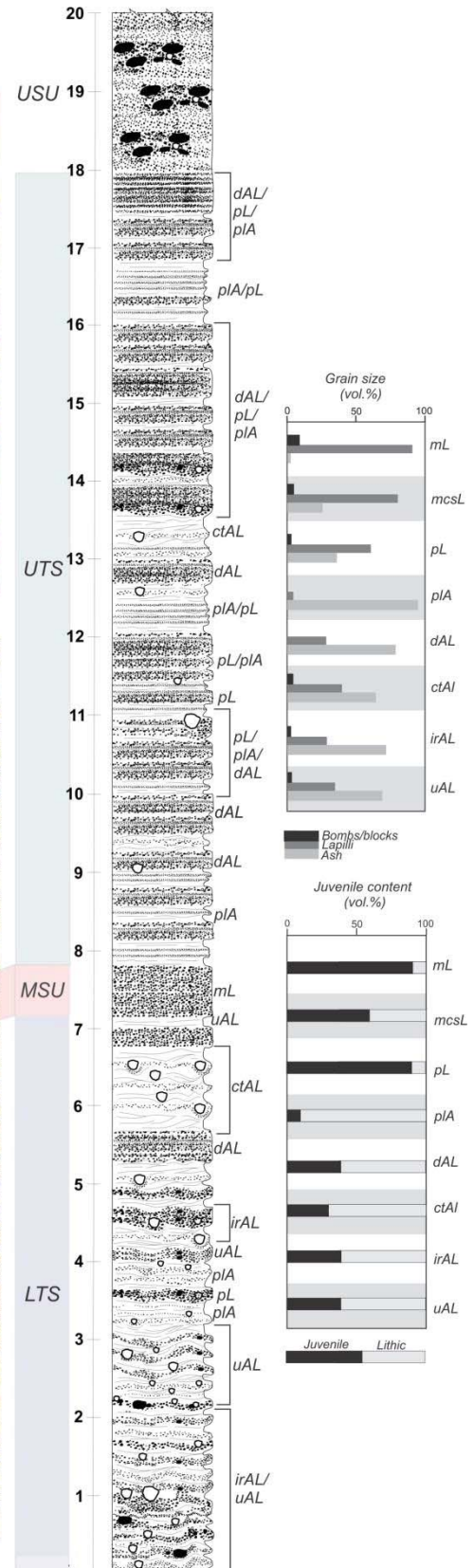
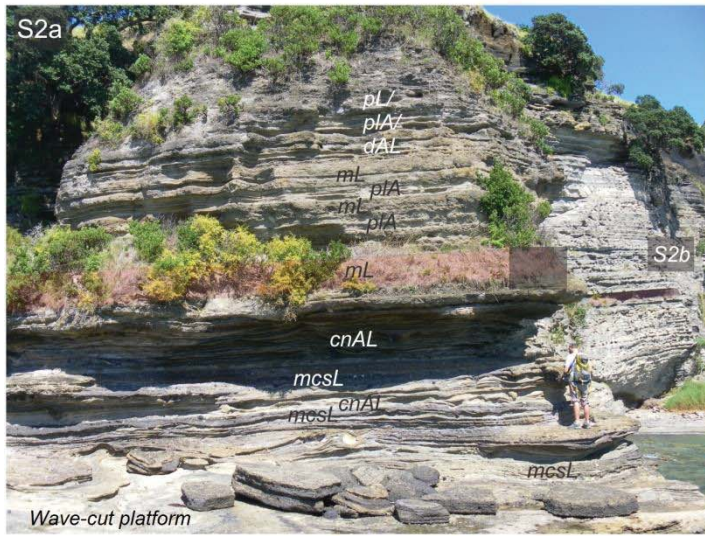


Fig. D.1.6 Sites S2a and S2b. Base of sequence at S2a intersects a wave-cut platform that marks approximately the highest tide sea level in the area. Base of sequence at S2b intersects the back beach level. Thickness of log (in metres) corresponds to thickness of sequence in photograph S2b. Person in picture S2a is 1.8 m high.

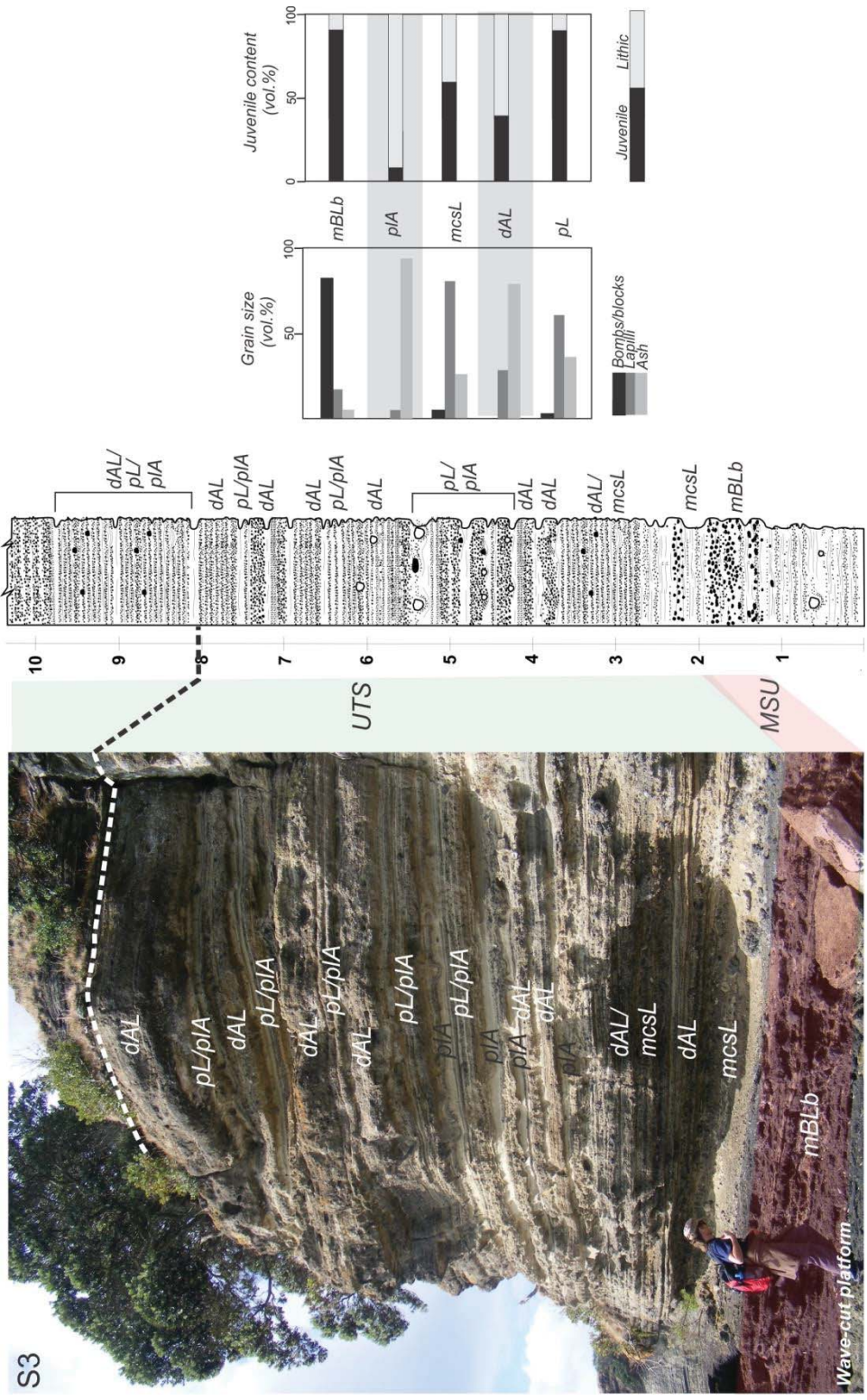


Fig. D.1.7 Site S3. Base of sequence intersects a wave-cut platform that marks approximately the highest tide sea level in the area. Thickness of log (in metres) corresponds to thickness of sequence of photograph.

D.1.2 Grain size distribution and juvenile/lithic content of Motukorea samples (chapter 6). These results are not presented in the chapter as explained in section 6.5.2 of chapter 6.

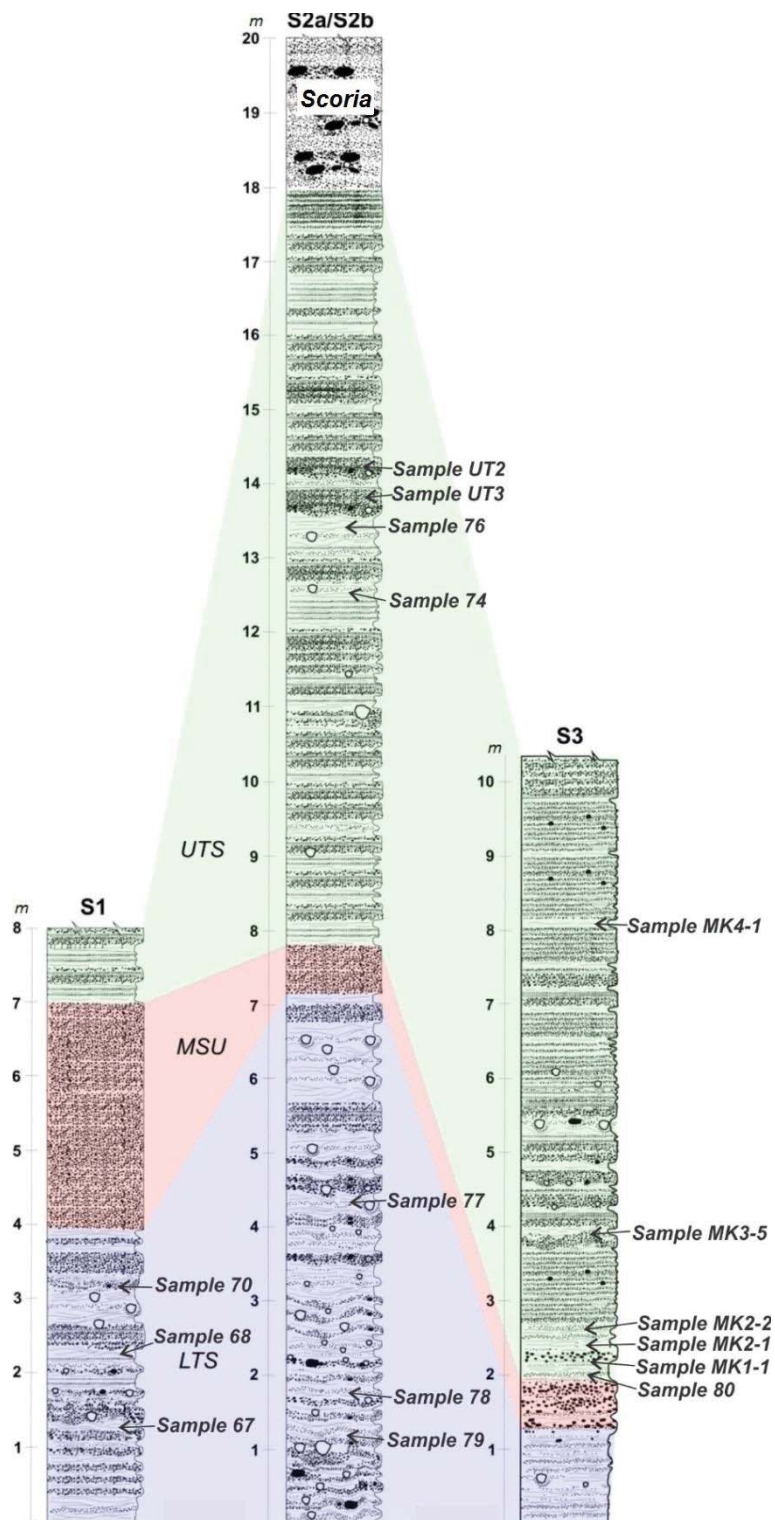


Fig. D.1.8 Location of sampling sites within the Motukorea sequence (for location of sites see Fig. D.1.1). Scale of logs indicates thicknesses. See Figs. D.1.3, D.1.6, and D.1.7 for details of stratigraphic logs.

Grain size	Phi	Samples / vol. %																
		67	68	70	74	76	77	78	79	80	MK2-1	MK2-2	MK3-5	MK4-1	UT2	UT3		
	-3.5														0.877095	1.635562		
	-3	1.680351			1.846038										3.622034	4.481007		
	-2.5	6.938359			4.703001	0.734118	0.626478			2.450548					3.605974	8.006672		
	-2	12.24316	4.143556	5.515954	10.83762	3.626981	3.496772			7.682798	6.456548				6.711633	11.3352		
	-1.5	14.5446	11.06036	11.54956	11.67902	3.612444	9.441923		6.442411	13.42723	18.51285	11.59715	12.28738	11.90175	11.54801	14.94211		
Medium Lapilli		35.40647	15.20392	17.06551	29.06568	7.973543	13.56517		6.442411	36.61692	45.86903	14.18108	33.10773	30.26608	26.36475	40.40055		
	-1	12.5452	15.04894	15.17312	11.57855	4.252072	11.04647	9.579277	9.104957	9.691805	12.8519	18.92167	10.67324	9.615468	14.65244	16.96977		
	-0.5	10.9061	14.26591	15.30041	10.25995	5.298735	9.154254	9.318498	11.73184	8.336277	8.904529	19.30824	9.562241	7.991116	16.71423	16.40761		
Fine Lapilli		22.63581	29.31485	30.47352	21.8385	9.550807	20.20073	18.89777	20.8368	18.02808	21.75643	38.22991	20.23548	17.60658	31.36666	33.37738		
	0	7.031948	8.727569	9.869314	8.068567	3.692397	6.737838	8.918637	9.538809	5.797421	6.150551	11.29196	7.202329	6.157732	13.70616	10.44702		
	0.5	5.087846	6.182708	7.5611	6.297878	2.122402	5.19082	9.179416	7.090218	5.024726	4.299266	7.548321	5.552434	5.713539	10.17184	6.633233		
	1	4.500787	5.88907	6.491853	5.607183	2.318651	5.216391	9.753129	5.877808	4.759802	3.687271	6.429298	5.445165	5.730958	7.837033	4.061826		
	1.5	3.488323	5	5.049219	4.621374	2.405873	4.660231	8.310153	4.802092	4.150477	2.922277	4.679552	4.663636	4.938379	3.449085	1.845694		
Coarse ash		20.1089	25.79935	28.97149	24.595	10.53932	21.80528	36.16134	27.30893	19.73243	17.05936	29.94914	22.86356	22.54061	35.16412	22.98777		
	2	3.269846	4.575856	4.296829	3.270439	3.909734	4.519899	10.10127	5.187071	2.3944	2.895068	3.688566	3.40238	3.453129	2.21621	1.108066		
	2.5	3.353401	4.475688	3.867511	3.958522	7.02782	5.386498	10.41234	7.5413	4.950615	3.542872	3.660186	4.390305	6.568666	1.559006	0.726796		
	3	3.862736	5.223638	3.795115	5.133574	10.10057	7.168268	10.12466	10.98907	3.050467	4.224149	4.156225	4.202815	5.088131	1.066103	0.391018		
	3.5	1.151946	1.574099	1.98235	2.027524	5.639729	2.7859	3.533977	4.218346	1.846406	1.324902	1.149457	1.439065	2.341211	0.744913	0.367189		
	4	1.760338	2.372412	2.050871	2.353396	7.489317	4.273988	3.463384	4.738935	2.355548	1.349387	1.575557	1.837475	2.807541	0.459549	0.220963		
Medium ash		13.39827	18.22169	15.60856	16.74345	34.16717	23.92724	37.63564	32.67472	14.59744	13.33638	14.22999	15.27204	20.25868	6.045782	2.814033		
	4.5	1.595406	2.081443	1.726726	1.869357	6.986461	4.349271	2.397724	3.465568	1.963338	0.869852	1.206204	1.525617	2.293734	0.447195	0.137561		
	5	1.127925	1.446964	1.152886	1.241542	5.39716	3.352908	1.41267	2.135505	1.348822	0.433421	0.68652	1.031729	1.548471	0.611496	0.282703		
	5.5	0.917809	1.192774	0.856912	0.936128	4.498303	2.639332	0.90749	1.557897	1.108219	0.23015	0.424565	0.831551	1.158509				
	6	1.049231	1.414882	0.893822	0.934004	4.832383	2.623358	0.734576	1.498781	1.31333	0.156107	0.344016	0.988241	1.122514				
	6.5	1.27237	1.781558	1.04714	0.996253	5.476616	2.754798	0.675559	1.514024	1.680749	0.122719	0.304932	1.292823	1.158456				
	7	1.130466	1.616848	0.945432	0.82137	4.708907	2.26029	0.528331	1.193686	1.572761	0.085704	0.221225	1.235841	0.934957				
	7.5	0.725679	1.044145	0.634095	0.509788	3.012751	1.353582	0.331801	0.723421	1.056758	0.049614	0.126351	0.841704	0.576237				
Fine ash (silt)		7.818885	10.57861	7.257012	7.308441	34.91258	19.30558	6.988151	12.08888	10.04398	1.947567	3.313812	7.747506	8.792879	1.058691	0.420264		
	8	0.375843	0.533854	0.349888	0.26605	1.606472	0.695952	0.185123	0.379454	0.56624	0.026347	0.063598	0.451162	0.3043				
	8.5	0.165449	0.22768	0.166379	0.121869	0.750356	0.316387	0.09442	0.179928	0.255265	0.00483	0.028985	0.200516	0.143766				
	9	0.075796	0.100705	0.081202	0.057834	0.36568	0.152499	0.037557	0.088956	0.118321		0.003537	0.090909	0.07199				
	9.5	0.01477	0.019186	0.026436	0.003134	0.134253	0.031087			0.041333			0.03105	0.01506				
Fine ash (clay)		0.631857	0.881425	0.623905	0.448887	2.856761	1.195926	0.3171	0.648337	0.981158	0.031177	0.09612	0.773638	0.535116				

Table D.1 Volume percentage values for phi fractions of selected sieved-Molukorea samples. The fractions are grouped in grain size grades. For location of samples see Fig D.1.8 above . Samples UT2 and UT3 are loose lapilli that belong to beds related to fall out inter-bedded with subile base surges (facies dAl and pl.).

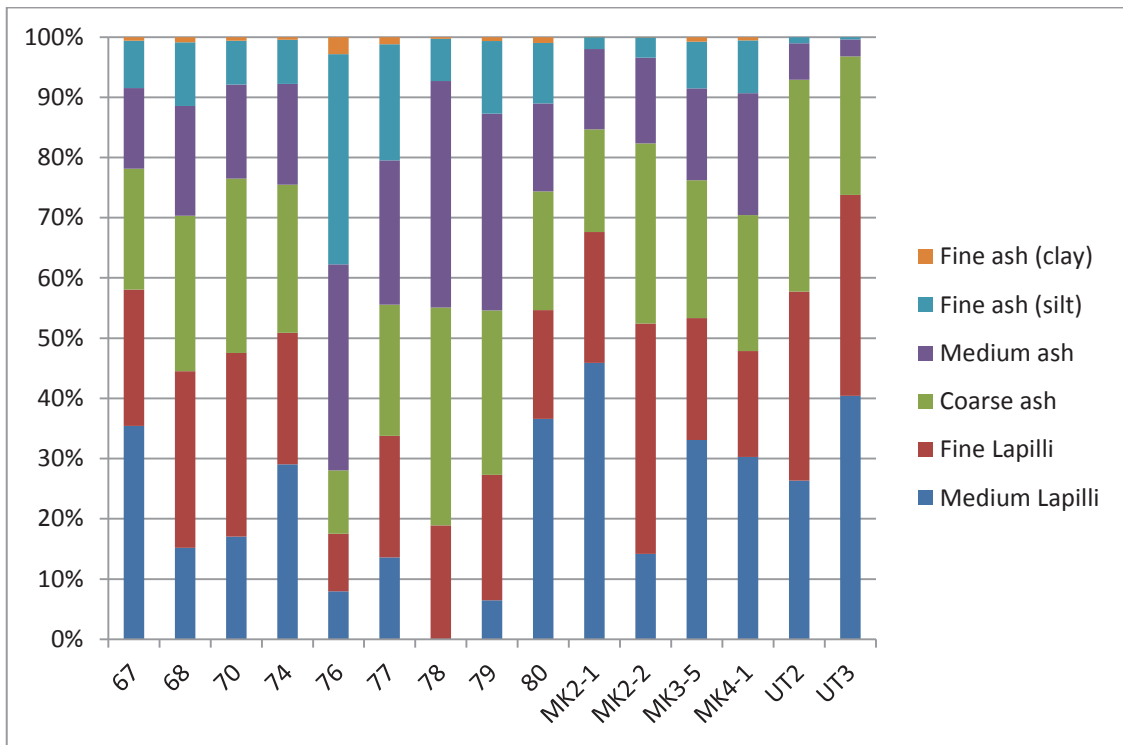


Fig. D.1.9 Graph representing values for grain size grades of Table D.1. For location of samples see Fig. D.1.8.

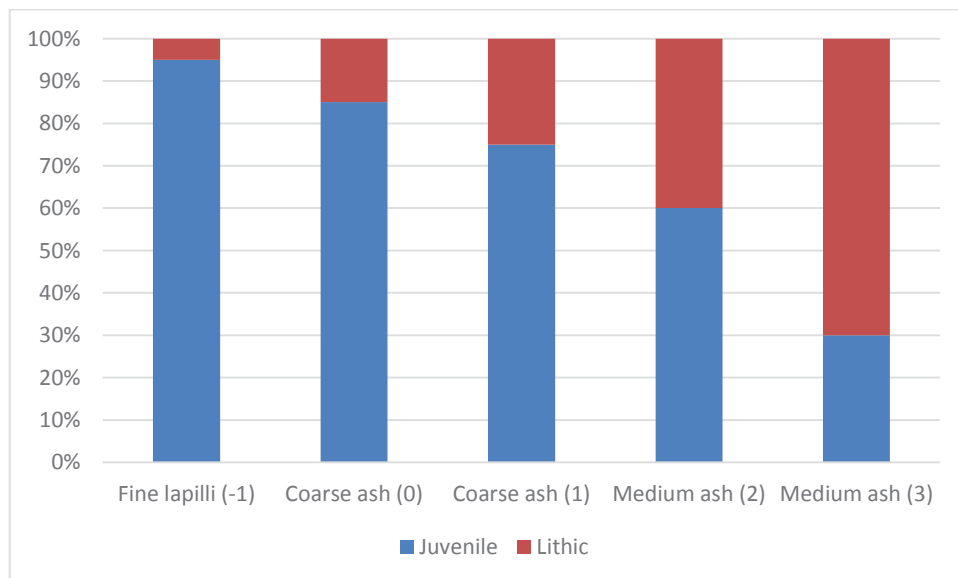


Fig. D.1.10 Graph showing the volume percentage of juvenile and lithic pyroclasts within a specific grain size grade. The number in parenthesis are the phi fractions corresponding to the grain size grade. For the volume percentages of grain size grades in the entire deposit see Table 6.1 in the text.

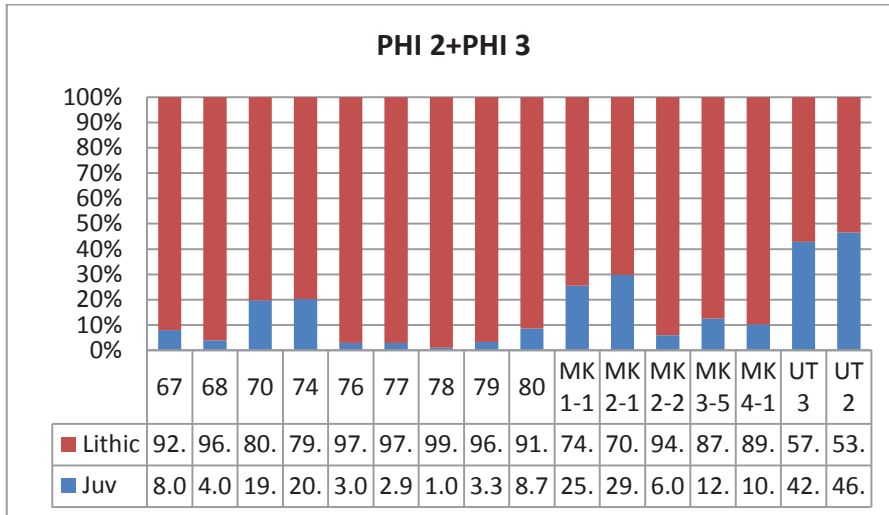


Fig. D.1.11 Lithic and Juvenile volume percentage for 2 and 3 phi fractions. Counts of 500 grains were performed. For location of samples see Fig. D.1.8. The presence of lithic grade fragments is greatly reduced in fractions >2 phi.

Appendix D.2 Lithofacies of Motukorea volcano

The sedimentary criteria to group and describe the lithofacies are provided in chapter 6. The referred figures for lithofacies are also displayed in chapter 6. The summarized information of these lithofacies is presented in Table 6.2 in chapter 6. The vol.% for grain size represents the approximate volume percentage of grain size within lithofacies

Clast-supported and juvenile-rich lithofacies

Massive bomb/lapilli breccia (mBLb) (Fig. 6.7a). Up to 40 cm-thick. Grain size: Small bombs (up to 90 vol.%). Sedimentary characteristics: Proportion of juvenile to lithic: 9:1. Dominantly massive, poorly sorted, ungraded, consolidated beds. In some sections, fine the coarser juvenile fragments appear to be embedded in an incipient fine ash matrix. Few lithic of coarse size (small bomb to lapilli size).

Interpretation: Scarce of lithic fragments and coarse-juvenile-rich, poorly sorted beds suggest deposition by fall from magmatic activity. The degree of consolidation indicates that fragments were hot at the time of deposition.

Massive lapilli tuff (mL) (Fig. 6.7b). Thickness: From cm up to 3 m (very variable). Grain size: coarse and medium lapilli (70 to 90 vol.%), little ash. Proportion of juvenile to lithic: 9:1. Dominantly massive, moderately sorted, ungraded, moderately consolidated, laterally parallel, continuous beds with transitional boundaries. Palagonitization may be present in sections at lower altitude. Scarce lithic of lapilli size.

Interpretation: Ungraded, massive and moderately sorted layers of dominantly juvenile lapilli point to deposition by fall from magmatic activity. The degree of consolidation can be attributed to the deposition of fragments when still hot. However the presence of palagonitization in sections relatively located at lower levels (the more consolidated parts) could indicate post-deposition alteration.

Matrix supported dominantly, variable proportion of juvenile to lithic lithofacies

Massive to crudely stratified lapilli tuff (mcsL) (Fig. 6.7c). Thickness: Tens of cm (<1 m). Grain size: medium lapilli to coarse ash (up to 90 vol.%) (considering only the juvenile-rich sections of the sequence); lithic: lapilli size (<10 vol.%) (in the total sequence), ash (up to 90 vol.%) (considering only the lithic-rich sections). Proportion of juvenile to lithic is variable, but approximately 6:4. Sedimentary characteristics: Ungraded to crudely stratified, poorly sorted, consolidated beds whose thickness may vary laterally and may show basal scour surfaces. Some juvenile/lithic block/lapilli are either embedded within the beds or form shallow impact structures. Scarce accretionary lapilli.

Interpretation: Poor sorting, relatively massive beds with coarse fragments embedded, and scour surfaces at their base imply dense, relatively erosive pyroclast density currents (high shear stresses at their basal boundary) with high sedimentation rates where turbulence and flow segregation was not relevant. Impact structures and accretionary lapilli indicate some water during deposition.

Parallel bedded lapilli tuff (pL) in combination with parallel bedded lapilli/ash (plA) (Fig. 6.7d). **pL:** Thickness: <1 m. Grain size: medium lapilli to coarse ash (>40 vol.%). Proportion of juvenile to lithic 9:1. **plA:** Thickness: <1 m. Grain size: medium to fine ash (>90 vol.%). Proportion of juvenile to lithic 1:9. In combination these two lithofacies reach few meters in thickness. Sedimentary characteristics: Poorly consolidated, rhythmic sequences composed by the combination of juvenile-rich (lapilli/coarse ash) with lithic-rich (ash) layers with sharp, but gradational boundaries. Layers are continuous laterally and individually have varied thicknesses. Juvenile-rich layers are usually reversed graded and moderately sorted, whereas lithic strata are non-erosive,

non-graded and laminated (include cross-lamination). Scarce subtle plastic deformation by coarser juvenile/lithic clasts is present.

Interpretation: Reverse grading of juvenile-rich layers with moderate sorting are related to deposition from grain flows that originated from rapidly falling pyroclasts from a cloud related to magmatic activity. Laminated nature of lithic-rich layers and some presence of juvenile trains indicate low sedimentation rate from turbulent diluted base surges with tractional flow boundaries, but the lack of scour and truncation characteristics suggest flows with low shear stresses. Subtle plastic deformation attests to the presence of some water in the deposition process.

Matrix supported, lithic dominated lithofacies

Diffusely bedded ash/lapilli (dAL) (Fig. 6.7e,b). Thickness: decimetres. Grain size: ash (lithic) (>60 vol.%); lapilli (juvenile) (<40 vol.%) (within the whole sequences). Proportion of juvenile to lithic: 4:6. Sedimentary characteristics: Diffusely stratified, poorly sorted, poorly consolidated ash beds with continuous trains of juvenile lapilli. The lapilli trains may show reverse grading and in some sections the trains thin upwards, as well as the grain size of the juvenile lapilli. The beds may be relatively plane parallel to slightly wavy and vary in thickness laterally. The bottom of these beds may define bed-load structures.

Interpretation: Crude bedding, diffuse stratification, and reverse grading of juveniles suggest tractional flow boundaries in turbulent base surges with relatively high rate of deposition. The lack of erosive boundaries suggests flows with low shear stresses at the basal boundaries.

Laminated ash (IA). Thickness: cm to dm. Grain size: ash (lithic) (>90 vol.%). Proportion of juvenile to lithic: 1:9. Sedimentary characteristics: Laminated, moderately sorted, poorly consolidated ash beds. They may contain subtle trains of juvenile, coarse ash. Cross lamination is present. Beds are laterally continuous and their thicknesses remain relatively constant, but may be deformed by impacts of coarse lithic/juvenile clasts. The bottom of these beds do not show erosive boundaries.

Interpretation: Overall well developed lamination points to low rates of sedimentation and high rate of deposition of dilute base surges. Cross lamination indicates transport in the turbulent regime, but the lack erosive boundaries suggest low shear stresses. Soft deformation suggests the presence of water during deposition.

Cross-stratified ash/lapilli (ctAL) (Fig. 6.7f). Thickness: decimetres. Grain size: ash (lithic) (>60 %); lapilli (juvenile) (<40 vol.%). Proportion of juvenile to lithic: 3:7. Sedimentary characteristics: Consolidated dune bedforms with internal layers lying at low angles (<20°) on both sides. Height of dune bedforms is <0.5 m and their length within a range of 2 m. Dune bedforms are usually stoss-side truncated and aggraded. Some dune bedforms show lensoidal shapes on the lee-side section with accumulation of coarser fragments towards the bottom. Laterally, dune bedforms may show symmetrical or random distribution. The sequences are formed by a rhythmic alternation of lithic-rich (ash) with relatively juvenile-rich (fine lapilli) layers. The former may exhibit reverse grading. Dune bedforms may be plastically deformed by block/bomb/coarse lapilli size fragments (both of juvenile and lithic), and show basal erosive boundaries.

Interpretation: Cross-stratification indicates transport in the turbulent regime of dilute base surges with tractional flow boundaries. The presence of well-developed beds containing reversed graded, coarser juvenile fragments suggest that flow segregation and a basal flow characterized by traction mechanisms may have been relevant. Truncation and erosive basal boundaries point to flows with high shear stresses, whereas some soft deformation characteristics are related to the presence of water during deposition. The presence of normally graded, lensoidal structures indicates the deposition of coarser clasts at flow margins of granular flows.

Convolved, cross-bedded ash/lapilli tuff (cnAL) (Fig. 6.7g). Thickness: 1-1.5 m. Grain size: ash (lithic) (>60 vol.%); lapilli (juvenile) <40 vol.%. Proportion of juvenile to lithic: 3:7. Sedimentary characteristics: This consolidated lithofacies share similar sedimentary characteristics as **ctAL**, but dune bedforms show clearly more evidence of soft deformation: impact structures, bed-load structures, and high angle undulations. The impact structures are caused by block/bomb/coarse lapilli size fragments (both juvenile and lithic).

Interpretation: Cross-stratification indicates transport in the turbulent regime of dilute base surges with tractional flow boundaries. The presence of well-developed beds containing reversed graded, coarser juvenile fragments suggest that flow segregation and a basal flow characterized by traction mechanisms may have been relevant. Truncation and erosive basal boundaries point to flows with high shear stresses, whereas some soft deformation characteristics are related to the presence of water during deposition. The presence of normally graded, lenticular structures indicates the deposition of coarser clasts at flow margins of granular flows. Pervasive soft deformation characteristics are related to the presence of relatively abundant water during deposition.

Crudely stratified, irregularly bedded ash/lapilli (irAL) (Fig. 6.7h). Thickness: ~1 m. Grain size: ash (lithic) (>60 vol.%); lapilli (juvenile) (<40 vol.%). Proportion of juvenile to lithic: 4:6. Sedimentary characteristics: Poorly consolidated, poorly sorted, rhythmic sequence formed by the combination of juvenile-rich (fine lapilli) and lithic (ash) layers. Individual layers subtly pinch and swell and are relatively continuous laterally. Juvenile-rich layers contain lithic lapilli, show reverse/normal grading, crude cross lamination, and may form faint lense-type structures. Also, they may exhibit subtle "ripple-type" undulations. Lithic layers may show cross lamination and subtle juvenile (fine lapilli)-rich layers. Coarse lapilli/block/bomb fragments do not usually form impact structures, but are embedded within the beds. In some parts these fragments show disorganized diffuse bedding or lenses. Contacts between layers are gradational.

Interpretation: Separation of upper finer material from reversed graded, lower, coarser material indicates flow segregation in flows characterized by a denser basal flow where tractional were dominant. Cross lamination suggests that the upper diluted part of the flow travelled in the turbulent regime at low rates of sedimentation. The virtual absence of erosive basal surfaces and the relatively plane parallel bedding point to low shear stress of relatively low energy flows.

Undulating, cross-laminated ash/lapilli (uAL) (Fig. 6.7i). Thickness: dm. Grain size: ash (lithic) (>60 vol.%); lapilli (juvenile) (<40 vol.%). Proportion of juvenile to lithic: 4:6. Sedimentary characteristics: This lithofacies shares most sedimentary characteristics with **irAL**. The main difference is that **uAL** does not exhibit "ripple-type" structures and the lithic segments are thicker (up to 30 cm) than the juvenile layers (10-15 cm). In addition, the dune bedforms show symmetrical and rhythmic undulations. Height of "crests" is <40 cm and distance between crests is about 2 m. Block/bomb/coarse lapilli size fragments (both juvenile and lithic) form scarce subtle impact structures, otherwise they are embedded in the sequence without deforming beds. Contacts between layers are gradational.

Interpretation: Separation of upper finer material from reversed graded, lower, coarser material indicates flow segregation in flows characterized by a denser basal flow where tractional were dominant. Cross lamination suggests that the upper diluted part of the flow travelled in the turbulent regime at low rates of sedimentation. The virtual absence of erosive basal surfaces and the relatively plane parallel bedding point to low shear stress of relatively low energy flows. Thicker fine-ash beds and dune bedforms with symmetrical undulations suggest the presence of a thicker suspended load and more energetic flow in comparison to the base surges that formed **irAL**.

Appendix E.1 North Head stratigraphic logs, frequency histograms, grain size distribution and juvenile/lithic content of selected samples.

E.1.1 North Head stratigraphic logs, frequency histograms

This appendix first presents the total of logs corresponding to North Head volcano (Figs. E.1 to). There are 2 extra logs included (PH1-B and PH3-B). The logs showed in chapter 7 (PH1, PH2, PH3, and PH4) are also included.

Fig. E.1. shows the plan view of North Head volcano. Alongside the 4 sites described in chapter 7, other 2 sites are included (PH1-B, PH3-B).

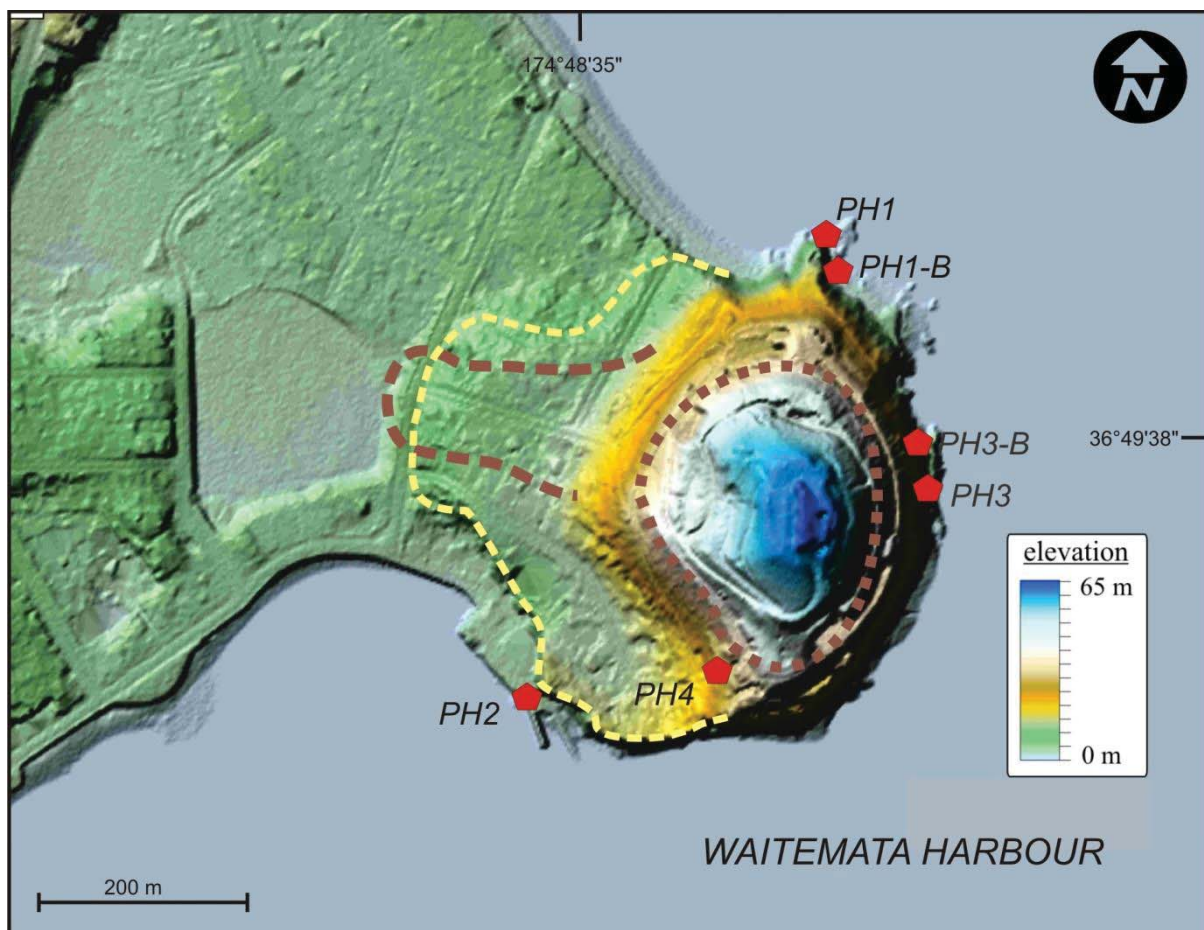


Fig. E.1. Location of sites

The stratigraphic logs are presented in the order showed in chapter 7 (from NH1 to NH4). All histograms show grain size distribution of the 11 sample numbers on Table E.1. Sample number is shown in histograms as *NH-number*. Lithofacies of sequences are described in section 7.5.2 and Table 7.2 in chapter 7.

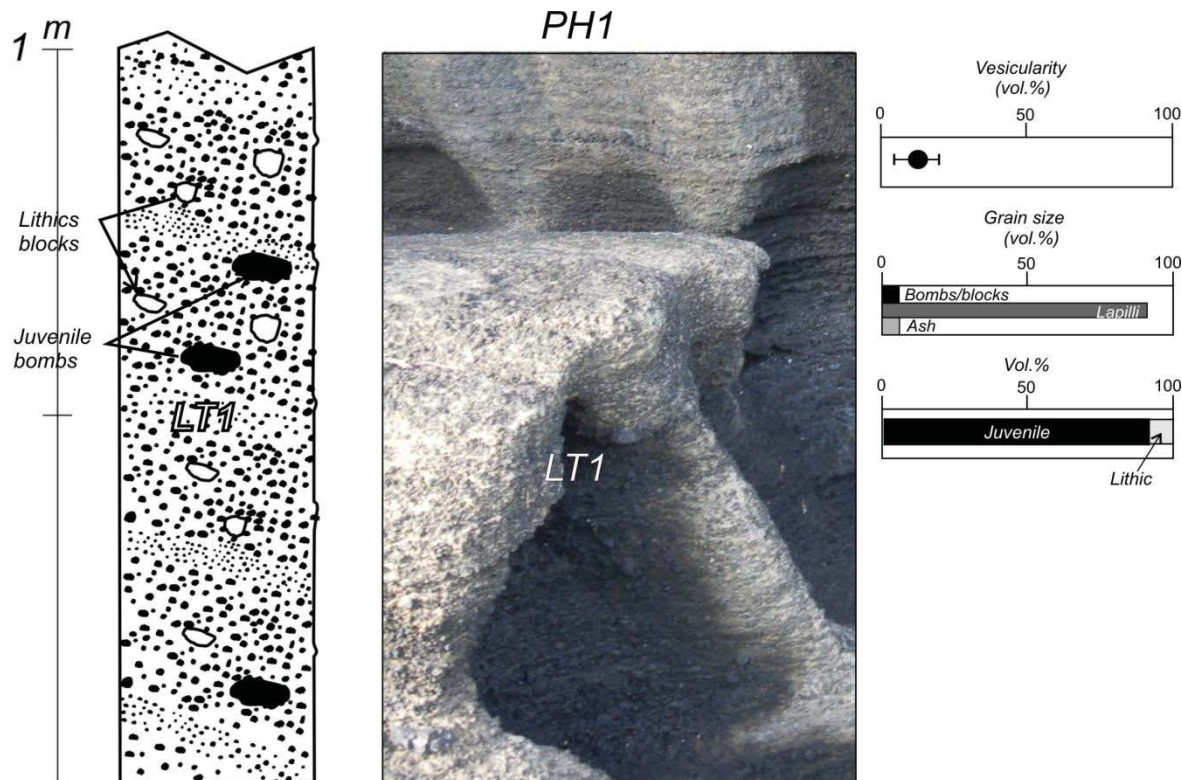


Fig.E.2 Site PH1. The picture represents a segment of an approximately 4 metre-thick sequence. Base of exposed sequence is approximately at Chart Datum which is approximately Lowest Astronomical Tide (from data in nautical chart 5322, Land Information New Zealand). Part of the sequence lies beneath reduced Chart Datum.

Fig. E.3 exhibits a wider view of the sequence at site PH1.



Fig. E.3 Bag is approximately 0.5 m-high. The whole sequence is constituted by lithofacies LT1.

PH1-B

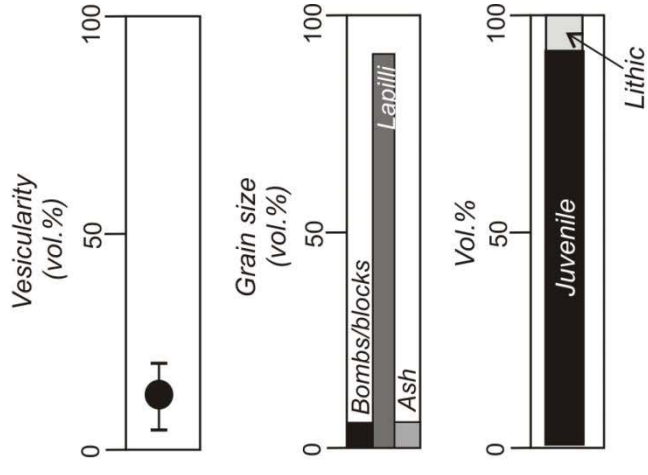
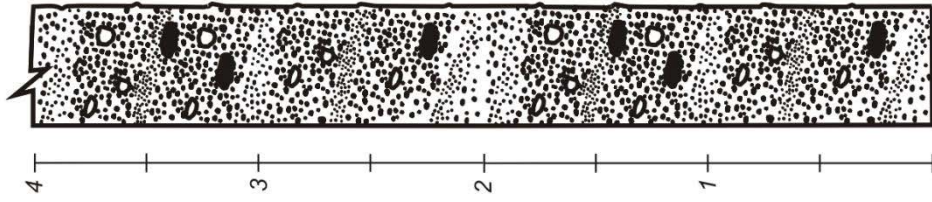


Fig. E.4. Site PH1-B. Base of exposed sequence is approximately at 2-3 m above Chart Datum which is approximately Lowest Astronomical Tide (from data in nautical chart 5322, Land Information New Zealand). Scale indicates thickness in metres.

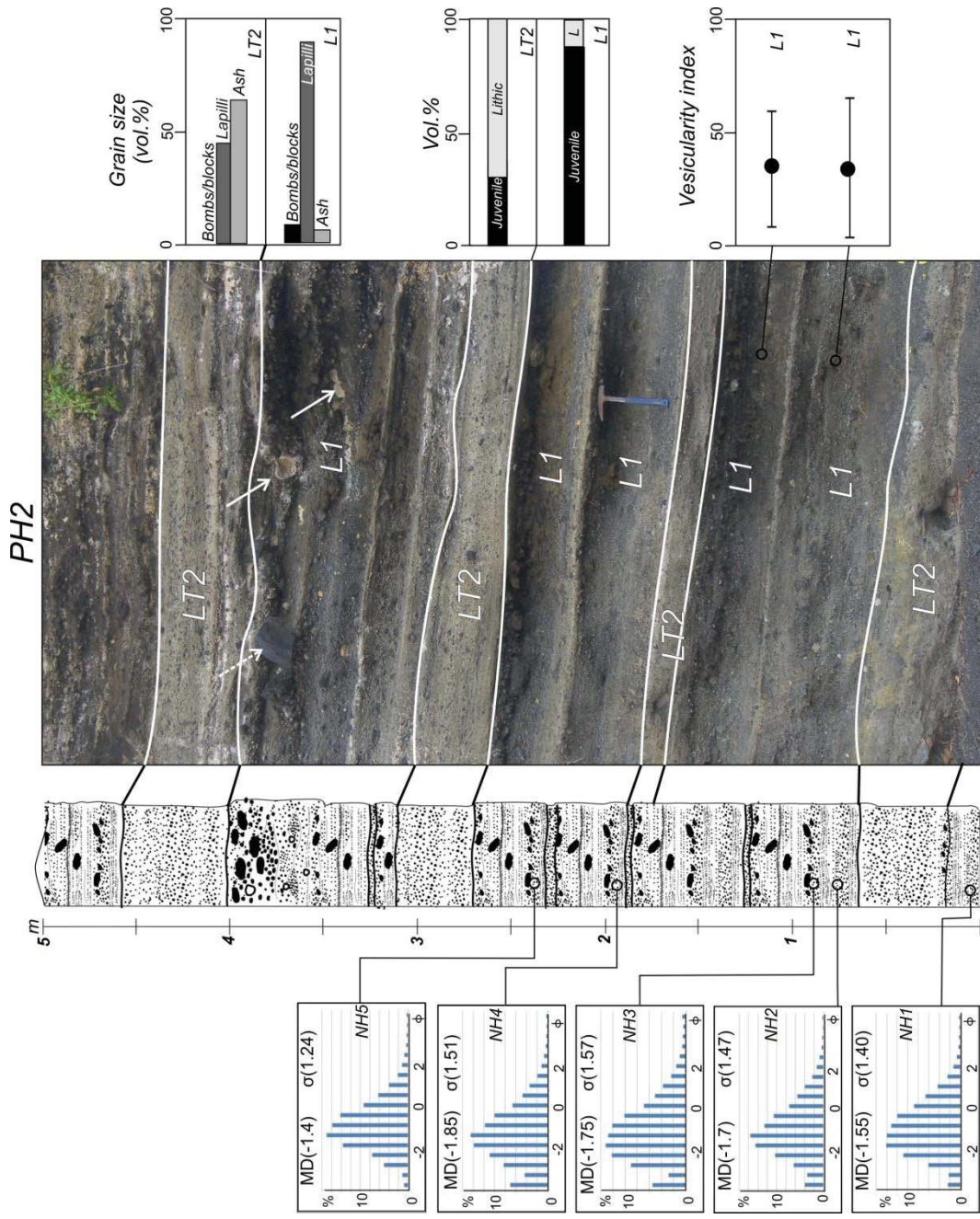


Fig. E.5. Site PH2. Base of exposed sequence is approximately 3-4 m above Chart Datum which is approximately Lowest Astronomical Tide (from data in nautical chart 5322, Land Information New Zealand). Scale indicates thickness in metres.

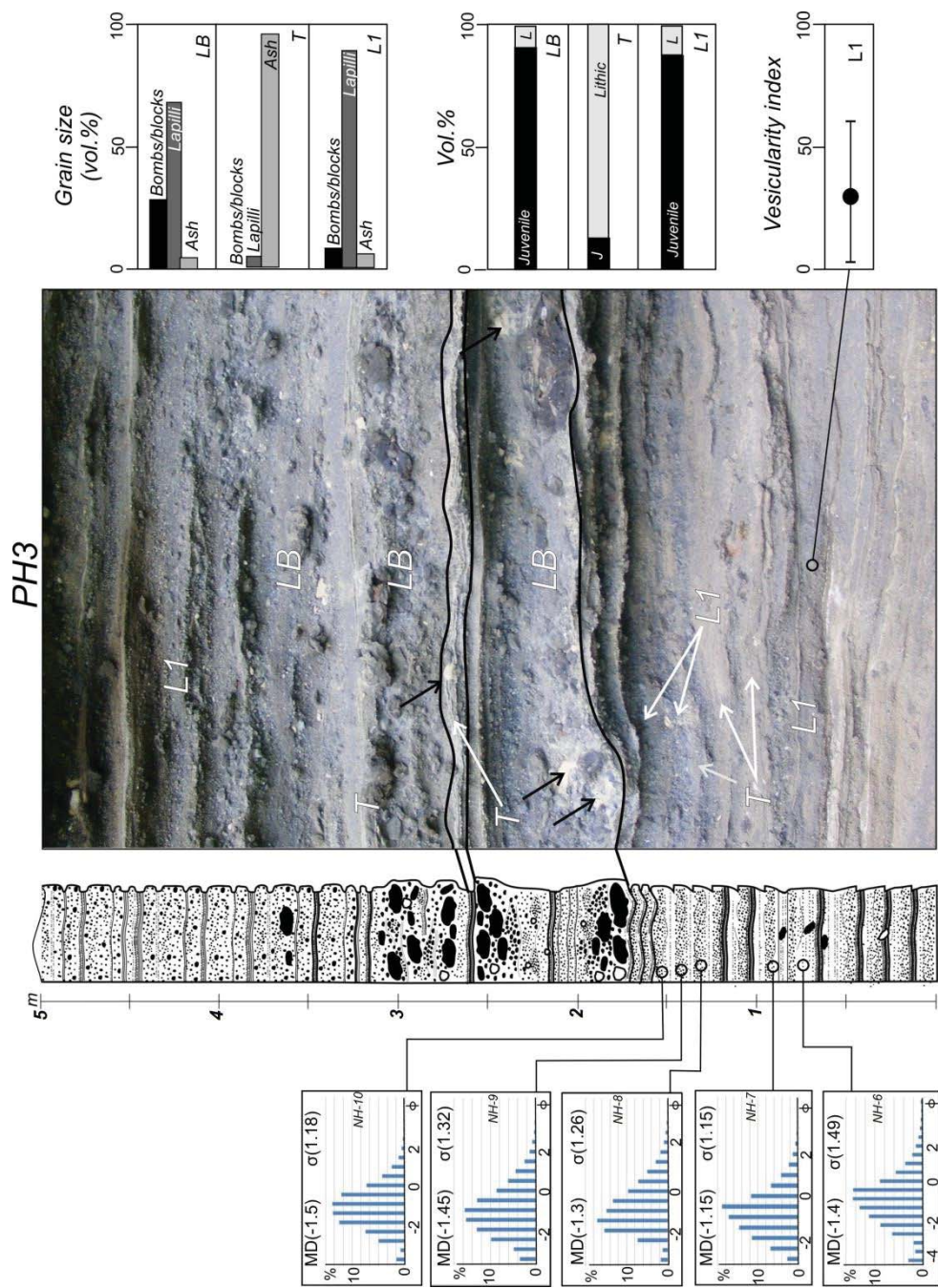


Fig. E.6. Site PH3. Base of exposed sequence is approximately at 7-8 m above Chart Datum which is approximately Lowest Astronomical Tide (from data in nautical chart 5322, Land Information New Zealand). Scale indicates thickness in metres.

PH3-B

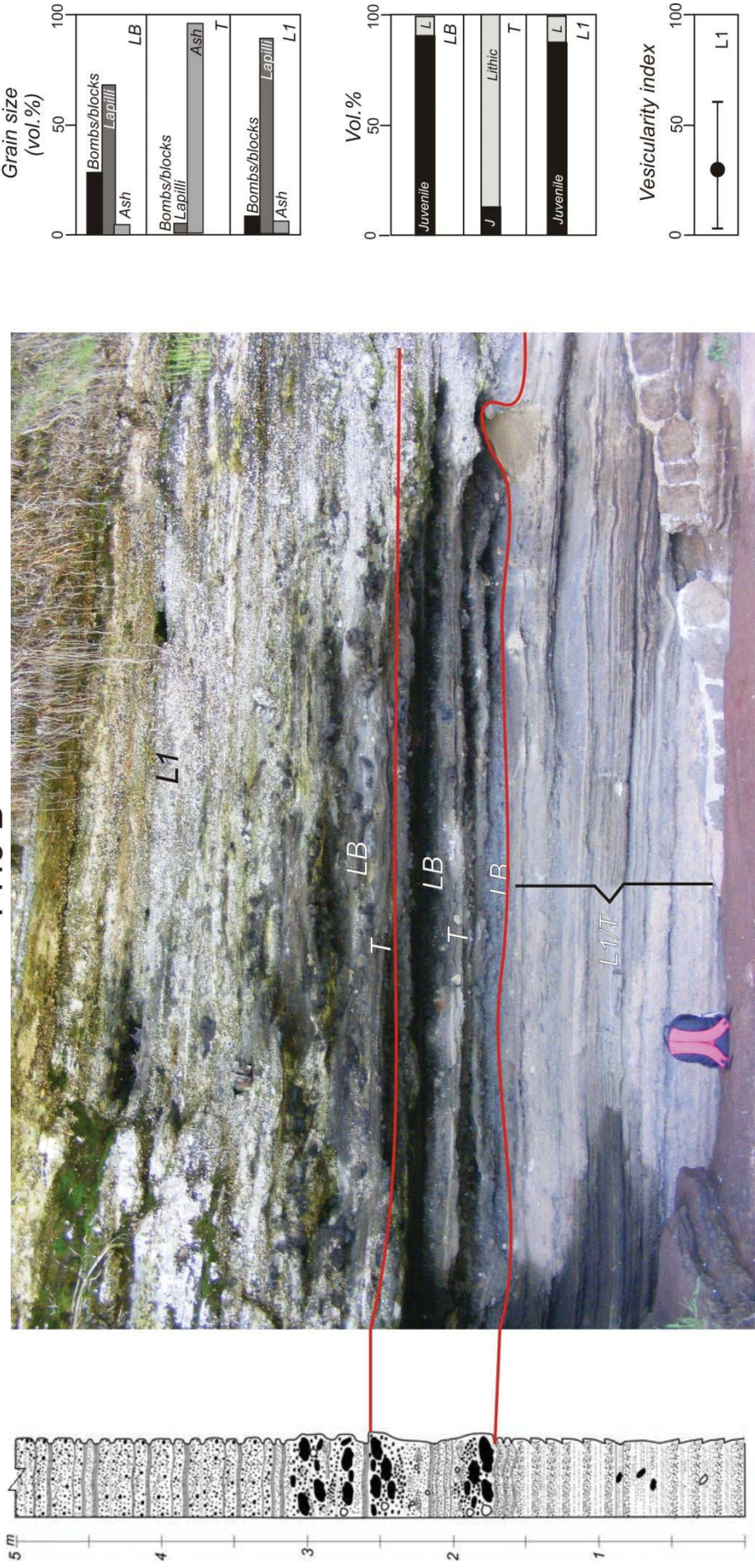


Fig. E.7. Site PH3-B. Base of exposed sequence is approximately at 5-6 m above Chart Datum which is approximately Lowest Astronomical Tide (from data in nautical chart 5322, Land Information New Zealand). Scale indicates thickness in metres.

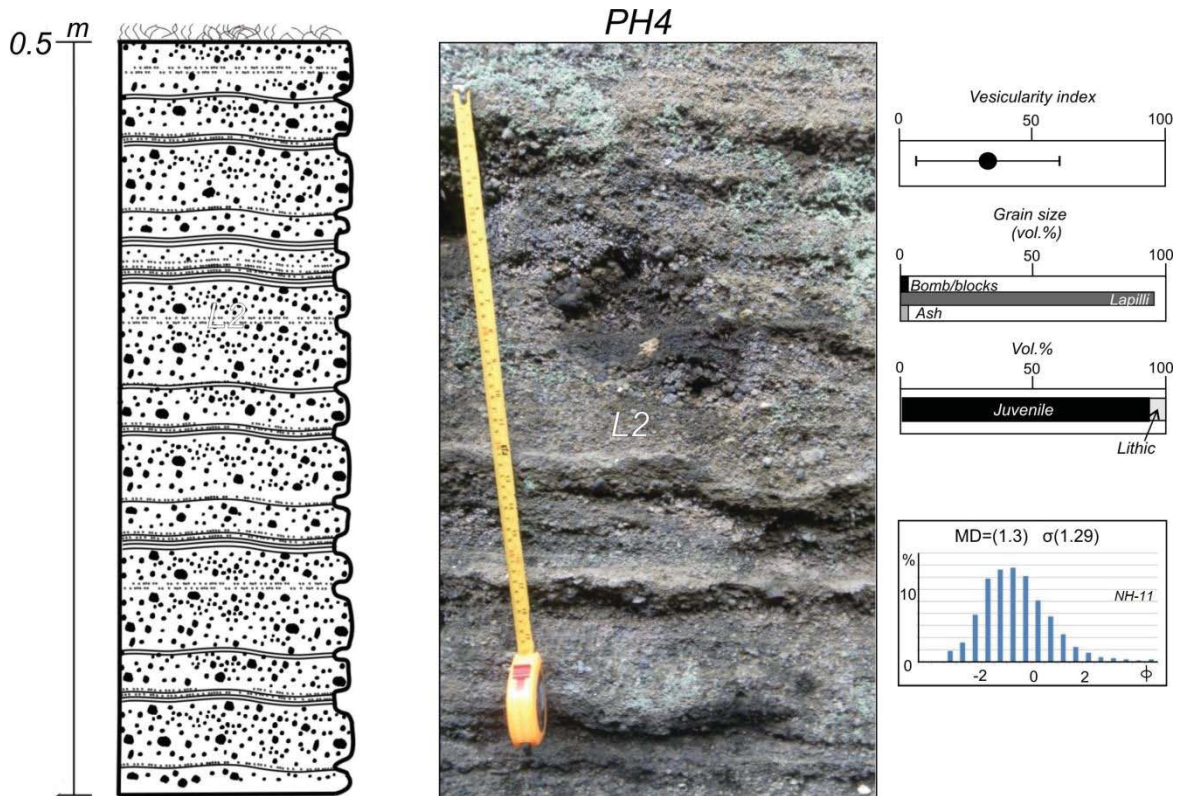


Fig. E.8. Site PH4. The picture represents a segment of an approximately 25 metre-thick sequence. Base of exposed sequence is approximately at 35-40 m above Chart Datum which is approximately Lowest Astronomical Tide.

E.1.2 Grain size distribution and juvenile/lithic content of selected North Head samples.

Table E.1 contain volume percentage values for phi fractions of selected sieved North Head-samples. The fractions are grouped in grain size grades. For location of samples see histograms in logs..

Grain size	Phi	Sample / vol.%										
		NH-1	NH-2	NH-3	NH-4	NH-5	NH-6	NH-7	NH-8	NH-9	NH-10	NH-11
	-4.5	0.00	0.00	0.00	0.00	0.00	3.05	0.00	0.00	0.00	0.00	0.00
	-4	2.38	3.97	5.47	7.04	0.79	1.55	0.00	0.00	0.00	1.91	
Coarse lapilli		2.38	3.97	5.47	7.04	0.79	4.60	0.00	0.00	0.00	1.91	0.00
	-3.5	2.24	3.44	2.80	4.29	1.18	1.89	0.00	1.71	3.52	0.99	1.79
	-3	6.05	6.34	9.02	8.26	5.01	6.39	2.67	1.31	4.85	5.96	3.19
	-2.5	10.84	10.32	12.22	10.89	7.48	8.84	6.88	7.36	9.87	8.94	7.80
	-2	14.12	14.53	13.21	13.92	13.65	11.19	11.55	15.37	13.00	14.89	13.76
	-1.5	13.98	15.64	12.75	14.47	17.06	13.22	14.69	17.14	15.35	16.33	15.26
Medium lapilli		47.23	50.27	50.00	51.82	44.37	41.53	35.79	42.90	46.60	47.10	41.80
	-1	13.15	12.60	12.10	11.80	15.89	14.57	17.29	14.87	15.64	16.45	15.55
	-0.5	12.04	10.61	10.08	9.96	14.21	14.55	18.92	13.32	12.93	14.45	14.19
Fine lapilli		25.19	23.21	22.17	21.76	30.10	29.12	36.21	28.19	28.57	30.90	29.74
	0	8.83	7.32	6.85	6.59	9.28	8.94	11.75	9.66	8.66	8.68	10.18
	0.5	6.64	5.57	5.05	4.73	6.25	5.66	6.74	7.20	6.14	5.16	7.48
	1	4.29	3.98	3.72	3.38	3.96	3.68	4.25	5.03	4.44	2.97	4.57
	1.5	2.42	2.40	2.38	1.91	2.14	2.21	2.31	2.94	2.48	1.41	2.46
Coarse ash		22.18	19.26	18.00	16.60	21.63	20.49	25.04	24.83	21.72	18.22	24.69
	2	1.30	1.43	1.53	1.14	1.26	1.46	1.32	1.82	1.38	0.77	1.49
	2.5	0.69	0.80	0.97	0.69	0.72	0.96	0.72	0.97	0.79	0.46	0.74
	3	0.37	0.40	0.55	0.34	0.40	0.60	0.38	0.59	0.37	0.27	0.56
	3.5	0.23	0.28	0.44	0.22	0.25	0.44	0.25	0.34	0.26	0.18	0.38
	4	0.18	0.17	0.33	0.17	0.20	0.33	0.14	0.18	0.14	0.06	0.21
Medium ash		2.77	3.07	3.83	2.55	2.83	3.79	2.81	3.89	2.95	1.74	3.37
	<4.0	0.24	0.21	0.52	0.23	0.28	0.46	0.15	0.19	0.17	0.13	0.39
Fine ash		0.24	0.21	0.52	0.23	0.28	0.46	0.15	0.19	0.17	0.13	0.39

Table E.1

The above data is presented as percentage of grain size grades in the following figure.

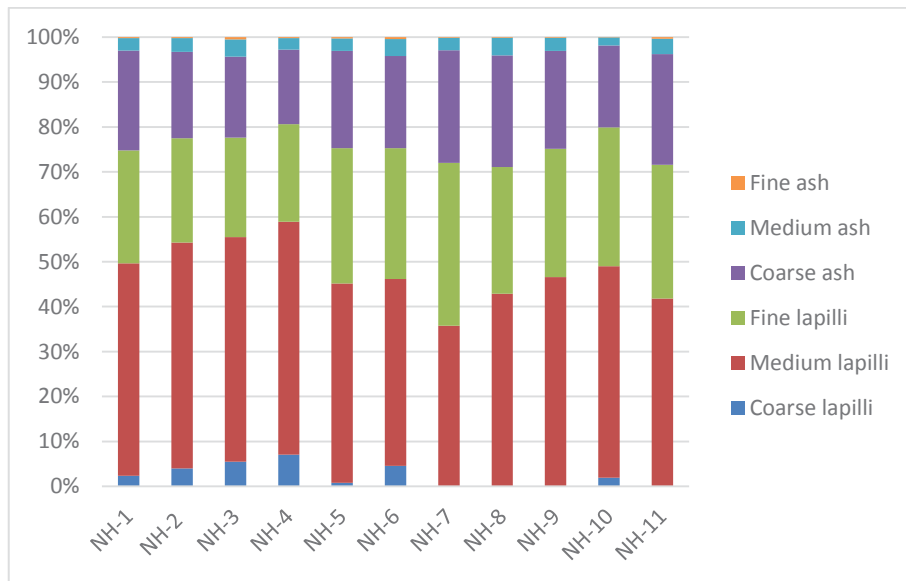


Fig. E.9 Graph representing values for grain size grades of Table E.1. For location of samples see histograms in logs.

Counts of 500 grains were performed for the same samples. The presence of lithic grade fragments is greatly reduced in fractions >2 phi.

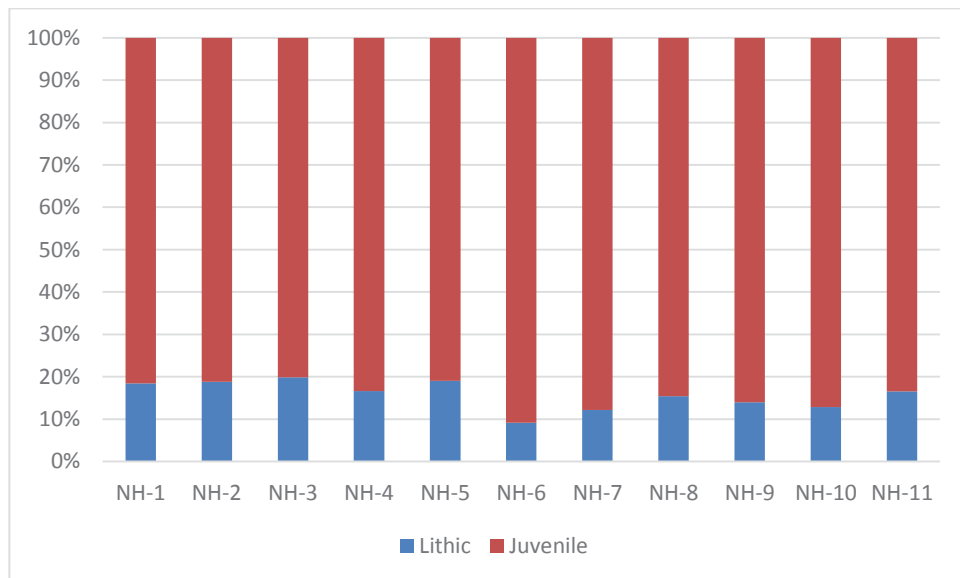


Fig. E.10 Lithic and juvenile volume percentage for 2 and 3 phi fractions.